Contributions to Mineralogy and Petrology (2023) 178:47
https://doi.org/10.1007/s00410-023-02029-5

ORIGINAL PAPER

U–Pb and trace element zircon and apatite petrochronology of eclogites from the Scandinavian Caledonides

Maciej Jaranowski[1] · Bartosz Budzyń[1] · Christopher J. Barnes[1] · Jarosław Majka[2,3] · Jiří Sláma[4] · Gabriela A. Kozub-Budzyń[3] · Karolina Kośmińska[3]

Received: 27 January 2023 / Accepted: 24 June 2023 / Published online: 10 July 2023

Abstract

The petrochronological records of eclogites in the Scandinavian Caledonides are investigated using EPMA and LA-ICPMS of zircon and apatite for U–Pb geochronology, combined with major and trace element characteristics. Metamorphic zircon from two eclogites from the Lofoten-Vesterålen Complex (Lofoten Archipelago region) collectively yielded a Concordia age 427.8 ± 5.7 Ma and an upper intercept U–Pb age 425 ± 30 Ma. Apatites from the same eclogites provided U–Pb lower intercepts at 322 ± 28 Ma and 354 ± 33 Ma, with the latter also yielding a younger age of 227 ± 24 Ma. Two eclogites from the Lower Seve Nappe (Northern Jämtland) demonstrate different zircon and apatite age records. Metamorphic zircon provided Concordia ages of 467.2 ± 5.9 Ma and 444.5 ± 5.5 Ma, which resolve the age of prograde metamorphism and zircon growth during retrogression, respectively. The lower intercept U–Pb ages of apatites from the same eclogites are 436 ± 18 and 415 ± 25 Ma, respectively. In combination with their geochemical characteristics, they suggest two separate stages of exhumation of eclogite bodies in the Lower Seve Nappe. Zircons from an eclogite from the Blåhø Nappe (Nordøyane Archipelago) yielded a continuum of concordant U–Pb dates from ca. 435 to 395 Ma, which suggests several cycles of HT metamorphism within short intervals. Distinctive trace element characteristics of apatites from the Blåhø Nappe eclogite suggest formation coeval with zircon and garnet during HT metamorphism, but Pb diffusion behaved as an open system until cooling during exhumation of the nappe at 390 ± 12 Ma (lower intercept U–Pb age of apatite). To summarize, this study presents the high potential of coupled zircon and apatite petrochronology of eclogites in resolving their metamorphic evolution, particularly with respect to using trace element characteristics of apatites to constrain the records of their growth, alterations and the meaning of their U–Pb age record.

Keywords Ultra-high pressure—(ultra) high temperature metamorphism · LA-ICPMS U–Pb isotopic dating and trace element analysis · Lofoten-Vesterålen Complex · Seve Nappe Complex · Blåhø Nappe

Introduction

The Scandinavian Caledonides offer an excellent geological setting to study tectono-metamorphic processes associated with subduction and continental collision due to their exceptional preservation and exposure of high-pressure (HP) and ultrahigh-pressure (UHP) eclogite-bearing terranes (Gee and Sturt 1985; Corfu et al. 2014). Investigating eclogites is especially advantageous as they are primary recorders of metamorphism during subduction/collision and later retrogression in various pressure–temperature (P–T) conditions. Their metamorphic records can be resolved in time by geochronological analysis of minerals such as garnet, zircon, rutile, ilmenite, titanite and apatite. As a result, a large number of orogenic evolution studies conducted within the

Communicated by Othmar Müntener.

✉ Maciej Jaranowski
ndjarano@cyf-kr.edu.pl

[1] Institute of Geological Sciences, Polish Academy of Sciences, Research Centre in Kraków, Senacka 1, 31002 Kraków, Poland

[2] Department of Earth Sciences, Uppsala University, Villavägen 16, 752 36 Uppsala, Sweden

[3] Faculty of Geology, Geophysics and Environmental Protection, AGH University of Science and Technology, Al. Mickiewicza 30, 30059 Kraków, Poland

[4] Institute of Geology, The Czech Academy of Sciences, Rozvojová 269, Prague 6 16500, Czech Republic

Scandinavian Caledonides have focused on eclogites and their metamorphic origin (e.g., van Roermund 1985; Kullerud et al. 1990; Cuthbert et al. 2000; Corfu et al. 2003a; Brueckner and van Roermund 2007; Smit et al. 2010; Root and Corfu 2012; Janák et al. 2013; Bukała et al. 2018; Fassmer et al. 2017, 2021). The use of zircon geochronology is limited by its availability in eclogite, but when present, zircon can offer a robust means to resolve the timing of various metamorphic events by combining U–Pb geochronology with trace element analysis (e.g., Corfu 2004; Corfu et al. 2014; Rubatto and Hermann 2007; Chen et al. 2010; Root and Corfu 2012). In contrast, apatite is a more common phase in eclogite, but there is little known regarding its chemical behavior in response to the metamorphic evolution of eclogites (e.g., March et al. 2022). Instead, studies of apatites from metamorphic rocks over the last few years have mainly focused on general characteristics of geochemical overprinting in low to high metamorphic conditions (e.g., O'Sullivan et al. 2018, 2020; Heinrichs et al. 2018, 2019). Thus, extending these records with regards to the evolution of eclogite is critical.

In this study, zircon and apatite were analyzed from eclogites in three different locations within the Scandinavian Caledonides, namely the Lofoten-Vesterålen Complex (Lofoten Archipelago), the Lower Seve Nappe (Northern Jämtland), and the Blåhø Nappe (Nordøyane Archipelago; Fig. 1). The P–T conditions of these locations are well established and their available geochronological data provide a good framework for further exploring the metamorphic history. The aim of this study was to extend our understanding of the tectonic evolution of eclogites using comprehensive zircon and apatite petrochronology, and to expand the knowledge of apatite behavior in eclogite. The coupled trace element and U-(Th)-Pb analyses of zircon

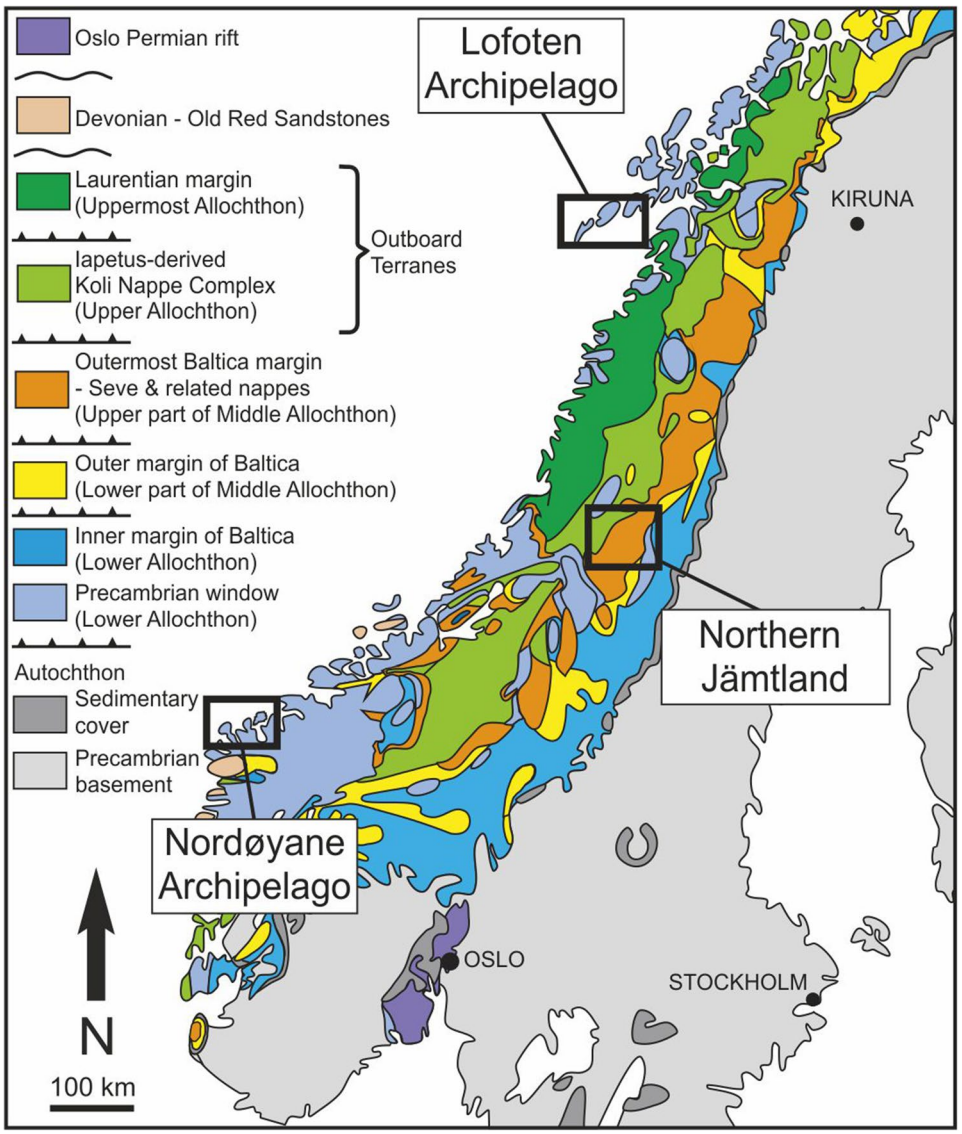

Fig. 1 Tectonostratigraphic map of the Scandinavian Caledonides (modified after Gee et al. 2013)

and apatite significantly increase the understanding of the tectonic evolutions of the studied localities in the Scandinavian Caledonides. This work also demonstrates the potential of combining apatite petrochronology with other geochronological studies in order to reconstruct different stages of the metamorphic evolution of (U)HP rocks and alteration processes that can occur in orogens.

Geological background

The Scandinavian Caledonides consist of numerous thrust sheets (Fig. 1) that altogether record the closure of the Iapetus Ocean, starting in late Cambrian time, which subsequently culminated in the Silurian to Devonian collision between Baltica and Laurentia (Gee 1975; Stephens et al. 1985; Stephens and Gee 1989; Roberts and Stephens 2000; Carswell et al. 2003; Torsvik and Cocks 2005; Gee et al. 2008, 2013; Corfu et al. 2014). Records of (U)HP metamorphism are predominantly retained within two tectonostratigraphic levels of the Scandinavian Caledonides: (1) the Precambrian window representing parautochthonous Baltican basement (Lower Allochthon), (2) the outermost Baltica margin (Middle Allochthon), namely the Seve Nappe Complex.

Baltican Basement at the Lofoten Archipelago

A prominent (U)HP locality in the parautochthonous Baltican basement is found in the Lofoten archipelago in Norway (Fig. 1; Markl and Bucher 1997; Steltenpohl et al. 2003, 2011a, b; Fournier et al. 2014, 2019). The basement rocks of the Lofoten archipelago consist of Neoarchean and Paleoproterozoic crystalline rocks collectively referred to as the Lofoten-Vesterålen Complex (LVC; Griffin et al. 1978; Corfu 2004). The Caledonian overprint of the LVC is not strong and eclogitization of the terrane is localized (e.g., Hacker et al. 2010). Eclogite within the LVC provided P–T conditions of 2.5–2.8 GPa and ~ 650 °C and Lu–Hf geochronology of the eclogite garnet yielded a Lu–Hf date of 399 ± 10 Ma, interpreted as the timing of HP metamorphism (Froitzheim et al. 2016). A dispersion of older Caledonian dates ranging from 513 ± 39 Ma to 449 ± 21 Ma was produced by zircon and titanite U–Pb geochronology of various intrusive rocks in the LVC, signaling an older Caledonian history of the LVC (Corfu 2004; Steltenpohl et al. 2011a, b). Single-grain white mica fusion $^{40}Ar/^{39}Ar$ geochronology has also yielded a large dispersion of dates from 781.3 ± 3.2 Ma to 299.6 ± 3.8 Ma, with the younger dates interpreted to represent exhumation of the LVC (Steltenpohl et al. 2011a, b).

The Seve Nappe Complex in Northern Jämtland

The Seve Nappe Complex extends for over 1000 km along strike of the Scandinavian Caledonides and bears multiple HP and UHP localities (e.g., Andréasson 1994; Gee et al. 2013). In northern Jämtland of Sweden, the Seve Nappe Complex is subdivided into the (U)HP rock-bearing Upper, Middle, and Lower Seve nappes (also referred to as the Eastern, Central, and Western belts; Trouw 1973; Williams and Zwart 1977; Zachrisson and Sjöstrand 1990; Janák et al. 2013; Gilio et al. 2015; Grimmer et al. 2015; Petrík et al. 2019). The Sjouten Unit in the Lower Seve Nappe (LSN) consists of eclogite, garnet peridotite and garnet pyroxenite hosted within metasedimentary rocks. Exposures at Tjeliken mountain and Stour Jougdan lake have been the focus for studying (U)HP metamorphism of the Sjouten Unit (van Roermund 1985, 1989; Litjens 2002; Bender et al. 2019). Recent work on eclogite and paragneisses at Tjeliken mountain have collectively yielded 2.5–2.7 GPa and 650–760 °C (Majka et al. 2014; Fassmer et al. 2017), whereas eclogite and garnet pyroxenite near Stour Jougdan lake have collectively provided 2.3–4.0 GPa and 750–960 °C (Klonowska et al. 2016).

Garnet Sm–Nd geochronology of an eclogite resolved metamorphism at Tjeliken mountain to 464 ± 9 Ma, which was reproduced by a garnet peridotite from Stour Jougdan lake that provided 460 ± 4 Ma (Brueckner and van Roermund 2007). Further zircon U–Pb geochronology of an eclogite at Tjeliken provided 445.6 ± 1.2 Ma, which was repeated by two single rutile U–Pb dates of 445.0 ± 2.4 Ma and 446.3 ± 3.7 Ma (Root and Corfu 2012). The results were interpreted to date the timing of eclogite-facies metamorphism with the previous Sm–Nd dates being the result of isotopic disequilibrium. However, the Sm–Nd dates were corroborated, and timing of eclogite-facies metamorphism refined, by zircon U–Pb geochronology of a paragneiss and garnet Lu–Hf geochronology of an eclogite at Tjeliken, which yielded 458.9 ± 2.5 Ma and 458.1 ± 1.0 Ma, respectively (Fassmer et al. 2017). Fassmer et al. (2017) speculated that younger U–Pb zircon ages determined by Root and Corfu (2012) were due to zircon growth or recrystallization during retrograde metamorphism related to fluid migration into the eclogite. The timing of eclogite-facies metamorphism of the Middle and Upper Seve nappes has also been resolved to the same time as the Lower Seve Nappe (Brueckner and van Roermund 2007; Grimmer et al. 2015). White mica $^{40}Ar/^{39}Ar$ and Rb–Sr geochronology applied to the Seve Nappe Complex resolved exhumation along crustal-scale shear zones at ca. 433–415 Ma (Grimmer et al. 2015; Bender et al. 2019).

The Blåhø Nappe in the Nordøyane Archipelago

The Nordøyane Archipelago exposes (U)HP rocks of the Baltican basement (part of the Western Gneiss Region of Norway) that are collectively referred to as the "Nordøyane UHP domain". The basement rocks are tectonically overlain by the Blåhø Nappe (Terry and Robinson 2003, 2004; Hacker and Gans 2005), which comprises eclogite hosted by garnet kyanite paragneiss, most prominently exposed on Fjørtoft. The nappe has typically been correlated with the Seve Nappe Complex, but recent work has revealed its tectonic origin to be distinct (Hollocher et al. 2022). Observations of Mesoproterozoic-aged inclusions of zircon and monazite within the garnets from the Fjørtoft paragneisses (e.g., Terry et al. 2000a; Cuthbert and van Roermund 2011; Liu and Massonne 2019, 2022; Walczak et al. 2019; March et al. 2022) and the Mesoproterozoic Lu–Hf dates obtained for garnet (Simpson et al. 2021; Tamblyn et al. 2022) lead to the assumption that the earliest garnet growth in samples from Fjørtoft predate the Caledonian Orogeny. The paragneiss has been reported to contain metamorphic microdiamond and assumed to record UHP metamorphism (Dobrzhinetskaya 1995), with original P–T conditions calculated at 3.4–3.9 GPa and ~ 820 °C (Terry et al. 2000a), which was revised and recalculated to 1.4–1.5 GPa and 770–820 °C (Liu and Massonne 2019, 2022; Gilio et al. 2021).

There have been several attempts at dating the timing of possible (U)HP metamorphism in the Blåhø Nappe. Terry et al. (2000b) produced concordant monazite U–Pb dates of 415.0 ± 6.8 Ma (for monazite included in garnet) and 398.2 ± 6.0 Ma (for matrix monazite) for the paragneiss. More recent monazite U–Pb geochronology from the gneiss produced an older concordia date of 431.1 ± 1.7 Ma from monazite included in garnet (Holder et al. 2015). The study also reported a spread of dates from ca. 425 Ma to 395 Ma and a concordia date of 393.0 ± 3.3 Ma for the youngest matrix monazite, which are similar to the results of Terry et al. (2000b). Zircon U–Pb geochronology of the gneiss yielded a concordia date of 446.6 ± 2.1 Ma, a spread of individual concordant dates from ca. 437 Ma to 423 Ma, and three younger concordant dates of 415.7 ± 2.4 Ma, 410.7 ± 2.0 Ma, and 397.0 ± 1.6 Ma (Walczak et al. 2019). Tual et al. (2022) reported zircon and monazite U–Pb ages of 450–370 Ma and a Lu–Hf garnet age of 422 ± 2 Ma. Altogether, the dispersion of the dates is interpreted to reflect either two separate episodes of HT metamorphism events, or they bracket two thermal excursions surpassing the solidus during a single protracted stage of HT metamorphism (Walczak et al. 2019). The youngest zircon dates of Walczak et al. (2019) have been reproduced by garnet Lu–Hf geochronology that yielded 404.5 ± 7.9 Ma, together interpreted to represent collision between Baltica and Laurentia (Cutts and Smit 2018; Walczak et al. 2019). Most recent U–Pb geochronology of rutile and monazite in metapelites from Fjørtoft provided concordant rutile dates ranging from ca. 449 to 378 Ma, as well as two populations of Caledonian-aged monazite at 423.2 ± 2.0 Ma and 385.2 ± 6.7 Ma (March et al. 2022). The older population ca. 423 Ma was interpreted as recording the early stages of (U)HP metamorphism, while the population ca. 385 Ma is consistent with past constraints for cooling in the region (Terry et al. 2000b; Krogh et al. 2011; Holder et al. 2015; March et al. 2022).

Sample selection and analytical methods

Sample selection

Five eclogite samples from three regions were selected for this study: samples LOF3/12, (68°06′16.1″N 13°16′09.3″E) and LOF11/12, (68°06′18.3″N 13°14′57.5″E) from the LVC, samples DG-TJ (64°33′21.5″N 14°43′21.8″E) and IK13-077 (64°35′41.9″N 14°51′37.4″E) from the LSN, and sample MB17.01E (62°42′45.1″N 6°25′28.4″E) from the Blåhø Nappe (Fig. 2). Sample selection criteria included regional diversity of the studied areas with previously constrained differences in the P–Tt evolution of the eclogites (Majka et al. 2014; Froitzheim et al. 2016; Fassmer et al. 2017; Walczak et al. 2019). All of the samples comprise well-preserved eclogite-facies mineral assemblages in mafic lithologies.

Sample preparation and analytical methods

In order to investigate the samples and conduct microanalysis, ca. 100 µm-thick sections were prepared from each of the sampled rocks. Furthermore, the eclogite samples were crushed and sieved to a fraction < 315 µm, followed by standard separation procedures involving Carpco and Frantz electromagnetic separators and heavy liquid density segregation. Zircon and apatite grains were hand-picked using a binocular microscope, mounted in epoxy, and polished to expose grain centers for laser ablation inductively coupled plasma mass spectrometry (LA-ICPMS) analyses. Quantitative mineral chemistry, back-scattered electrons (BSE) imaging were performed on carbon-coated thick sections (ca. 100 µm) and rounded 1-inch grain mounts using a JEOL SuperProbe JXA-8230 electron microprobe equipped with five wavelength dispersive spectrometers at the Laboratory of Critical Elements AGH–KGHM (AGH University of Science and Technology, Kraków, Poland). Analytical details of electron probe microanalysis (EPMA) measurements are presented in Supplementary Table S1.1. Data were corrected to the ZAF procedure using in-house JEOL software.

Representative portions of each sample were also milled for whole rock chemical analysis, which were performed

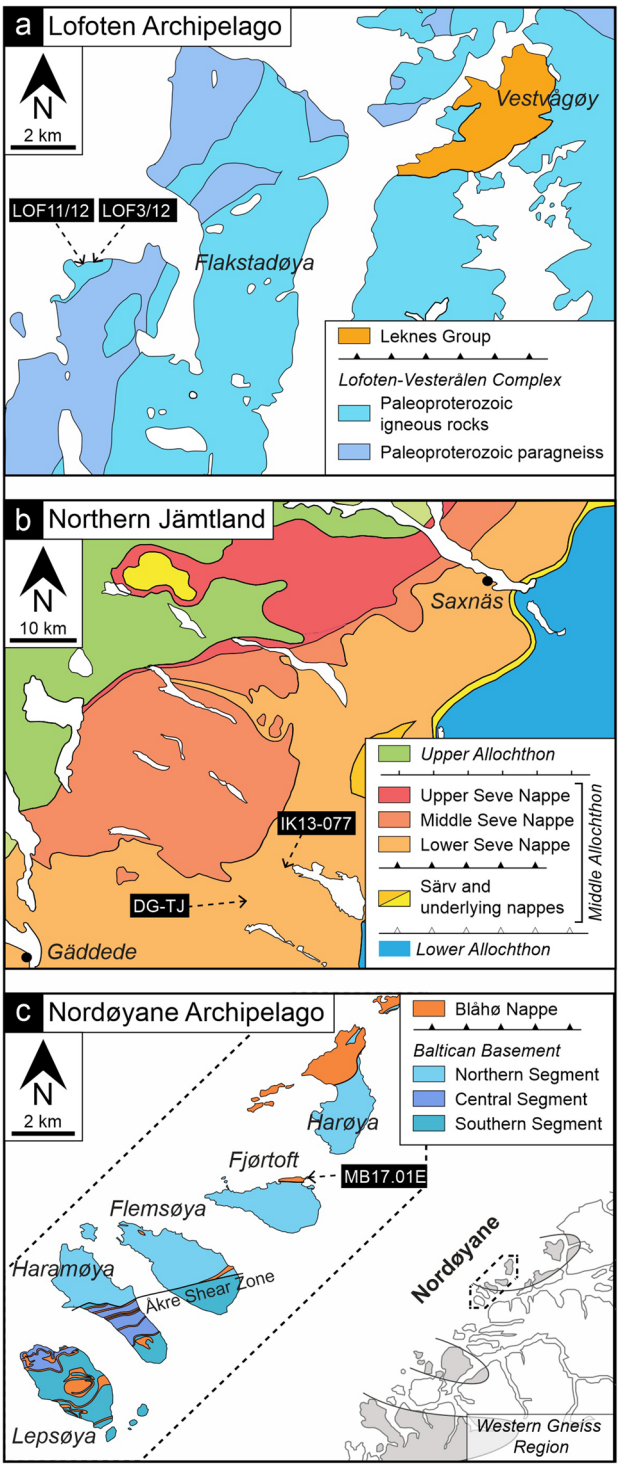

Fig. 2 Geological maps of **a** the Lofoten Archipelago (modified after Steltenpohl et al. 2006); **b** Northern Jämtland in Sweden (modified after Zachrisson and Sjöstrand 1990); **c** the Nordøyane Archipelago (modified after Terry et al. 2000b). Sampling locations are shown with labels in the black boxes

in the Actlabs Activation Laboratories, Canada. Major and trace element abundances were analyzed by ICP-MS following a lithium metaborate/tetraborate fusion and dilute nitric digestion. LOI was determined by weight difference after ignition at 1000 ℃. The complete dataset of whole rock geochemistry is presented in Supplementary Table S4.

Prior to the LA-ICPMS analyses, cathodoluminescence (CL) imaging was performed on the zircon grains using a JEOL JXA-8530F Field Emission EPMA at the Institute of Petrology and Structural Geology, Charles University in Prague. The CL images were used to couple trace element and U–Pb analyses in the same zones within the grains. U–Pb and trace element analyses of apatite and zircon were conducted in 1-inch grain mounts using a Thermo Scientific Element 2 sector field ICP-MS coupled to a 193 nm ArF excimer laser (Teledyne Cetac Analyte Excite laser) at the Institute of Geology of the Czech Academy of Sciences, Prague, Czech Republic. The analytical details are provided in Supplementary Tables S1.2–S1.5. Reproducibility and age uncertainty of reference material are propagated for all data involving the Concordia age calculation following the recommendation of Horstwood et al. (2016). No common Pb correction was applied to the data due to the high Hg contamination of the commercially available He carrier gas, which precludes accurate correction of the interfering ^{204}Hg on the low signal of ^{204}Pb. The U–Pb dates are presented as Concordia plots generated with ISOPLOT v. 4.16 (Ludwig 2012). Based on the Ti concentrations of zircon grains, temperatures of zircon formation were calculated using the calibration method described in Ferry and Watson (2007) using a_{SiO2} and a_{TiO2} values of 1.

Results

Sample description

The eclogite LOF3/12 exhibits porphyroblastic texture with porphyroblasts of garnet, omphacite and amphibole. The matrix is mostly composed of symplectitic intergrowths of plagioclase and clinopyroxene replacing the amphibole (Fig. 3a). Garnet porphyroblasts are subhedral and contain inclusions of quartz, amphibole, rutile and kyanite, with minor ilmenite, biotite and apatite. Small aggregates of iron oxides are omnipresent within the rock matrix. Rare individual subhedral grains of apatite (ca. 100 µm in size), as well as intergrowths of ilmenite and rutile, occur in the matrix.

Eclogite LOF11/12 shows porphyroblastic texture with garnet, amphibole, and omphacite porphyroblasts in the matrix, mostly composed of symplectitic intergrowths of secondary amphibole, clinopyroxene and plagioclase (Fig. 3b). Subhedral garnet porphyroblasts include quartz, omphacite, amphibole, rutile, apatite, kyanite, and iron

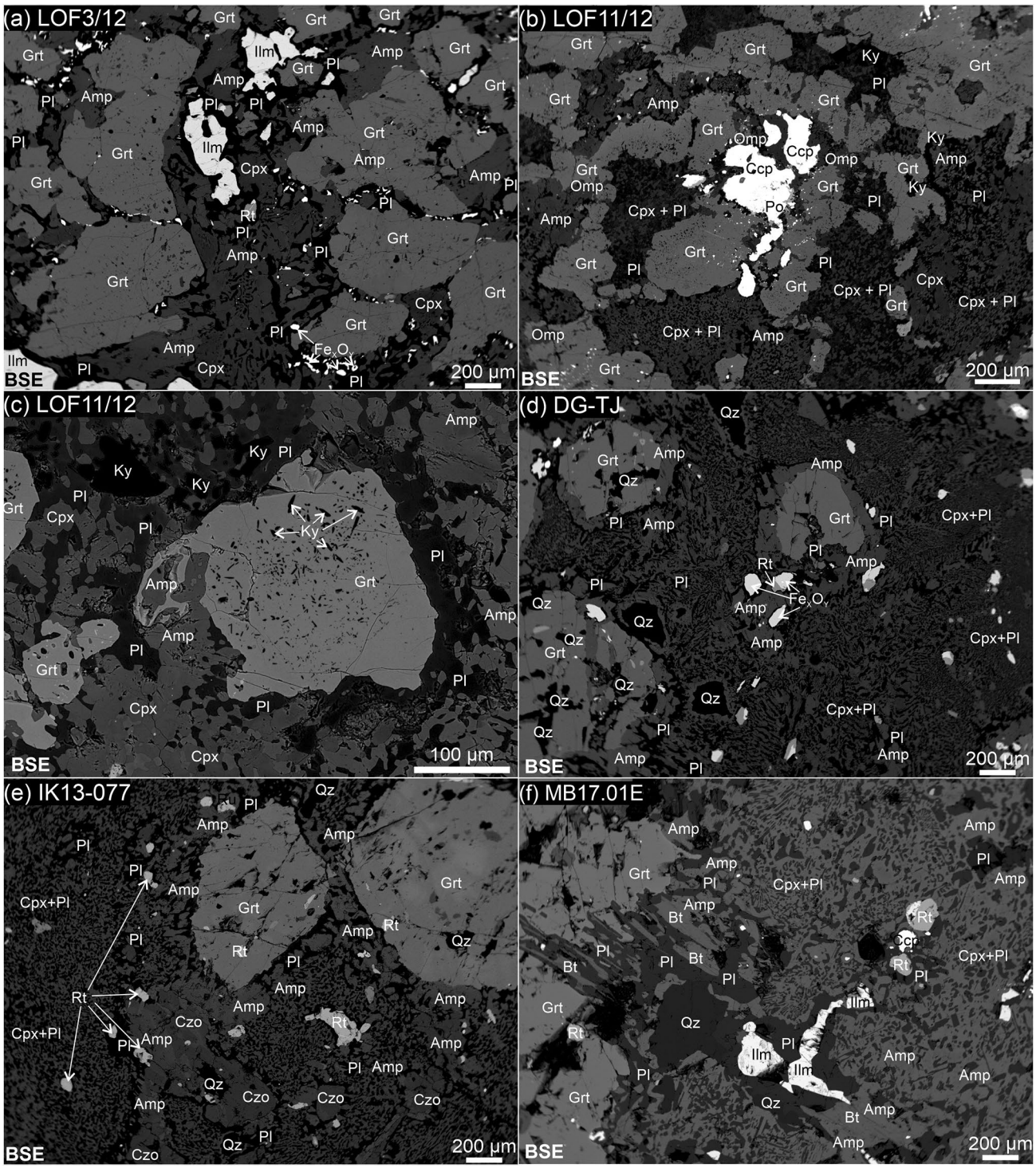

Fig. 3 BSE overview of the studied eclogites. *Amp* amphibole, *Bt* biotite, *Ccp* chalcopyrite, *Cpx* clinopyroxene, *Czo* clinozoisite, *Grt* garnet, *Ilm* ilmenite, *Ky* kyanite, *Pl* plagioclase, *Po* pyrrhotite, *Rt* rutile, *Ttn* titanite, *Qz* quartz

sulfides. Quartz, kyanite, and aggregates of iron sulfides and oxides occur in the matrix (Fig. 3b, c). The matrix amphibole shows compositional zoning with transition to clinopyroxene. Apatite occurs either as anhedral grains between garnets, or as subhedral grains within the matrix.

The eclogite DG-TJ exhibits porphyroblastic texture with garnet, amphibole, and omphacite porphyroblasts. Garnet forms euhedral to subhedral grains rimmed by secondary amphibole and plagioclase (Fig. 3d). Inclusions in garnet consist mostly of quartz, amphibole, rutile, ilmenite, and to the lesser degree, biotite and apatite. The matrix is dominated by symplectitic intergrowths of plagioclase and clinopyroxene with different sizes of blasts. Accessory phases in the matrix include commonly ilmenite and rutile, whereas iron oxides and sulfides, apatite, titanite, zircon, and epidote are rarer (Fig. 3d). Rutile, ilmenite, and small grains of zircon (ca. 20 µm) form intergrowths, but zircon also occurs as single grains within the matrix in close proximity to rutile and ilmenite (Fig. 4b). Titanite occasionally forms overgrowths on rutile and ilmenite, or anhedral grains in a short distance to these minerals (Fig. 4a, b).

The eclogite IK13-077 has porphyroblastic texture, composed of porphyroblasts of garnet, amphibole, and clinozoisite in a matrix of symplectitic intergrowths of amphibole, clinopyroxene, and plagioclase (Fig. 3e). Irregular grains of quartz occur in the matrix. Garnet forms euhedral to subhedral grains with delicate reaction-rims of plagioclase and amphibole, and inclusions of quartz, rutile, amphibole, and zircon. Iron sulfides and rutile, accompanied by apatite and zircon, are occasionally present in the matrix.

The eclogite MB17.01E exhibits porphyroblastic texture with large porphyroblasts of garnet and amphibole. Euhedral to subhedral blasts of garnet bear inclusions of quartz,

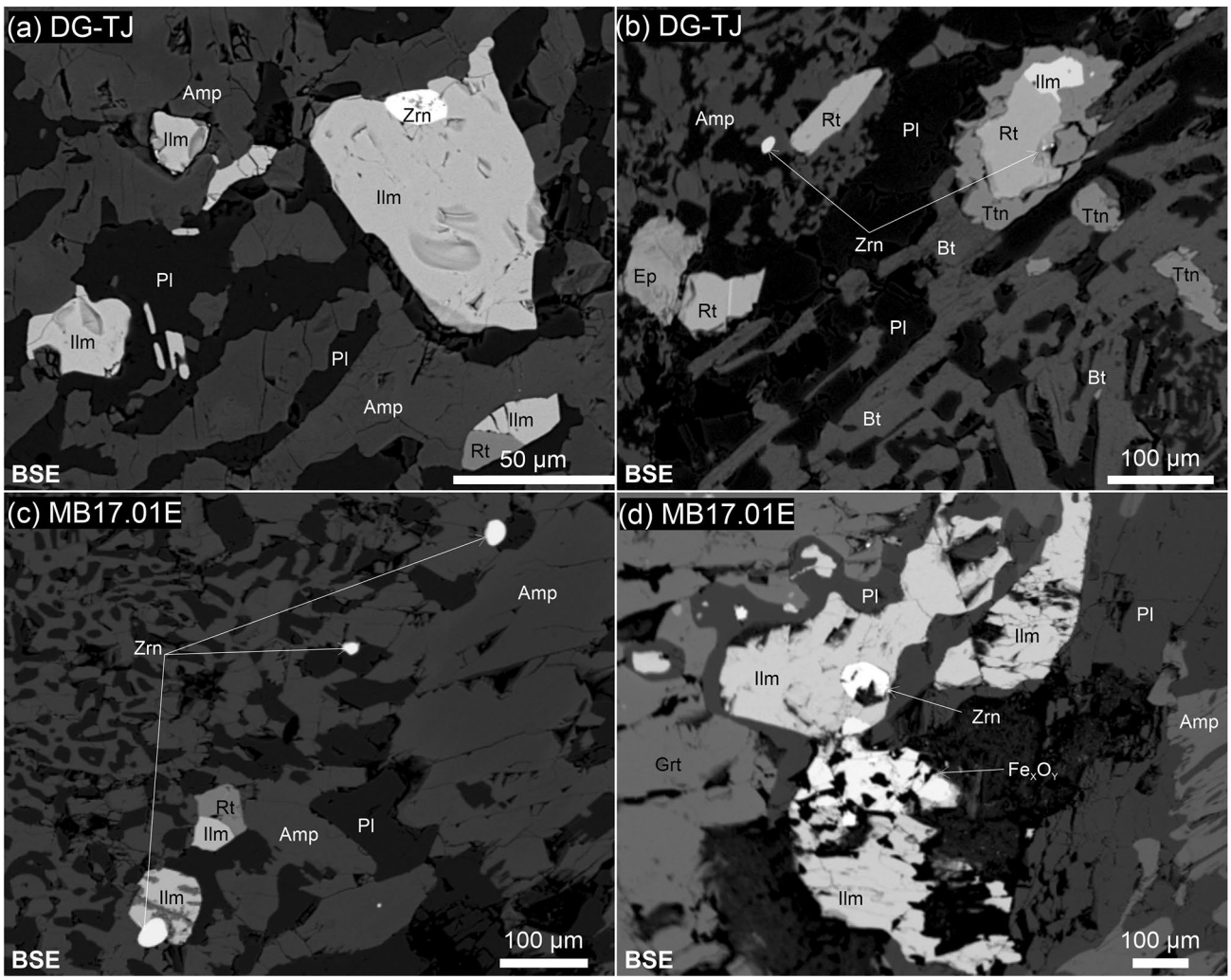

Fig. 4 BSE images of the eclogites DG-TJ (**a**, **b**) and MB17.01E (**c**, **d**) presenting textural relations of rutile (Rt) being replaced by the ilmenite (Ilm) and titanite (Ttn)

amphibole, rutile, ilmenite, biotite, clinopyroxene, apatite, iron sulfides, zircon, and calcite. Inclusions within garnet sometimes involve two or more phases intergrown with each other. Two types of symplectitic intergrowths are present in the matrix: linear symplectites of plagioclase–biotite (Pl–Bt) and irregular symplectites of plagioclase–amphibole–clinopyroxene (Pl–Amp–Cpx). The Pl–Bt type formed close to the garnet, whereas Pl–Amp–Cpx type forms most of the rock matrix (Fig. 3f). Accessory phases include ilmenite and rutile, which usually form intergrowths commonly accompanied by zircon (Fig. 4c, d), and less common iron sulfides and oxides, and apatite are present in the matrix.

Eclogites demonstrate variations in bulk composition from 44.33 to 54.01 wt.% SiO_2, 13.22–20.23 wt.% Al_2O_3, 8.84–20.65 wt.% $Fe_2O_3^{(T)}$, 5.71–9.02 wt.% MgO and 9.37–10.77 wt.% CaO (Supplementary Table S4). Chondrite-normalized trace element patterns of DG-TJ, IK13-077, and MB17.01E are generally similar with a slight slope from La to Lu ($(La/Lu)_N$ ratios of 2.09 to 3.03). The Lofoten samples LOF3/12 and LOF11/12 have lower concentrations of rare earth elements (REE, i.e. Y + La–Lu) and steeper slope ($(La/Lu)_N$ ratios of 6.06 to 9.32), with positive Eu anomalies (Eu/Eu* from 1.16 to 2.01).

Zircon

Lofoten-Vesterålen complex (Lofoten Archipelago)

Zircon from eclogite LOF3/12 forms anhedral to subhedral grains with sizes from 60 × 80 to 100 × 200 µm. In total, 40 grains were analyzed for trace element and U–Pb data, from which 20 trace element and 38 U–Pb analyses were accepted for further statistics. Most of the zircons show complex to irregular zoning, generally bright in CL imaging, sometimes with patches of oscillatory zoning. Some of the grains also exhibit dark domains in CL imaging with oscillatory zoning that have thin bright rims in CL imaging (Fig. 5a). The dark domains have higher concentrations of heavy rare earth elements (HREE, 215.8–1313.1 ppm) and Th/U ratios of 0.74–1.62 compared to brighter domains (22.6–99.4 ppm HREE, 0.01–0.02 Th/U), and yielded $^{207}Pb/^{206}Pb$ dates from 1750 ± 18 Ma to 1813 ± 22 Ma (n = 15, from − 1.9 to 6.2% disc.; Figs. 6a, 7a, 8a). Brighter domains yielded $^{206}Pb/^{238}U$ dates from 422 ± 5 Ma to 473 ± 6 Ma (from − 2.3 to 2.0% disc.), with two outliers of 517 ± 6 Ma and 685 ± 14 Ma (− 0.3% disc. and 24.2% disc., respectively) in partially altered zircons. Early Paleozoic grains form two populations of dates: an older one spanning from 473 to 449 Ma and a younger population providing a Concordia age of 427.8 ± 5.7 Ma (n = 10, 2σ, MSWD = 0.02; Fig. 6b, c). Crystallization temperatures for the zircon in the Lofoten samples were calculated at 621–775 °C with Ti-in-zircon thermometry (from < 2 to 30.7 ppm Ti; Supplementary Table S3.2).

Eclogite LOF11/12 has a very low abundance of zircon, resulting in investigation of only 5 grains (7 trace element and 11 U–Pb analyses were accepted). Zircon grains are anhedral or rounded, and ca. 60 × 100 to 90 × 140 µm in size (Fig. 5b). Four of the zircon grains exhibit core–rim textures with cores showing oscillatory or complex zoning and a darker contrast in CL imaging compared to the irregular, thin, and homogeneous rims. The oscillatory zoned cores have high HREE concentrations (258.9–1076.6 ppm), Th/U ratios of 1.04–2.38 and provide $^{207}Pb/^{206}Pb$ dates of 1767 ± 5.7 Ma to 1792 ± 15 Ma (− 0.3–5.7% disc., Figs. 6d, 7b). One remaining zircon grain exhibits a slightly darker rim compared to its core (Fig. 5b) and has lower concentrations of HREE (21.7–46.5 ppm) and Th/U ratios of 0.01–0.13 (Fig. 8b). The zircon yielded three $^{206}Pb/^{238}U$ dates of 395 ± 4 Ma (1.8% disc.), 411 ± 4 Ma (0.5% disc.) and 421 ± 5 Ma (0.2% disc.) with an intercept age 425 ± 30 Ma (Fig. 6e).

Lower Seve Nappe (Northern Jämtland)

Zircon from eclogite DG-TJ forms subhedral to anhedral grains of 40 × 50 to 80 × 130 µm in size. The grains show oscillatory to sector or, rarely, irregular complex zoning. In total, 33 grains were analyzed for trace element and U–Pb characteristics, from which 20 trace element and 32 U–Pb analyses were accepted. Zircon grains are bright in CL images with occasional dark cores with irregular zoning and 10–50 µm in size. One zircon has a dark core (ca. 100 µm-sized) with a convolute zoning, and a thin and homogeneous bright rim (Fig. 5c). The large core was the only dark domain analyzed, providing a high concentration of HREE (2916.5 ppm), Th/U ratio of 1.12 and $^{206}Pb/^{238}U$ date of 524 ± 6 Ma (1.2% disc.; Figs. 6f, 7c). The bright domains of zircons from DG-TJ sample are characterized by HREE concentrations varying between 33.1–173.4 ppm and low Th/U ratios 0.01–0.04. The $^{206}Pb/^{238}U$ dates form a tight cluster 440 ± 5 Ma to 456 ± 7 Ma (− 2.7–1.3% disc.), which provide a Concordia age of 444.5 ± 5.5 Ma (n = 26, 2σ, MSWD = 0.01; Fig. 6g). Several zircon domains produced outlier results with $^{206}Pb/^{238}U$ dates from 392 ± 4 Ma to 500 ± 9 Ma (− 0.7–3.8% disc.), higher Th/U ratios of 0.09–1.56, and elevated content of light rare earth elements (LREE, Figs. 7c, 8c) which are probably related to alteration or a mixed analysis of core (hidden below the sample surface) and rim. Ti-in-zircon temperatures of 620–698 °C were calculated for the bright zircon domains (from < 2 to 8.6 ppm Ti; Supplementary Table S3.2).

Zircon grains from eclogite IK13-077 are elongated and subhedral with sizes of 50 × 80 to 100 × 280 µm. In total, 29 grains were analyzed resulting in acceptance of 20 trace element and 42 U–Pb analyses. The zircons show distinct core–rim relations with oscillatory-zoned

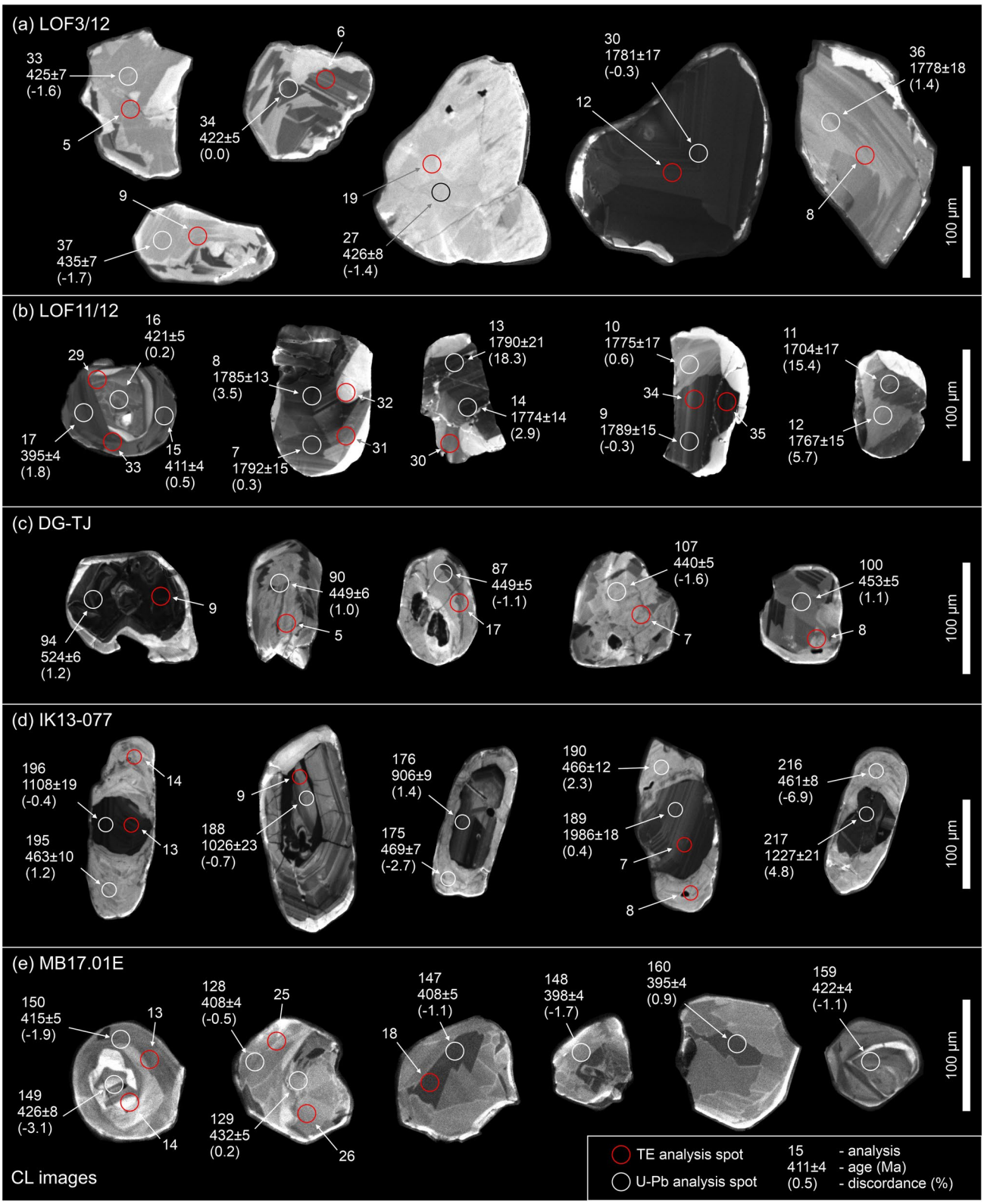

Fig. 5 CL images of representative zircon grains from investigated eclogites. LA-ICPMS analytical spots are marked for the trace element and U–Pb measurements. Presented U–Pb data (white spots) include spot number, $^{206}Pb/^{238}U$ date for data < 1000 Ma and $^{207}Pb/^{206}Pb$ date for data > 1000 Ma with ± 2σ error (Ma) and discordance (%) in brackets. Red spots—trace element measurements

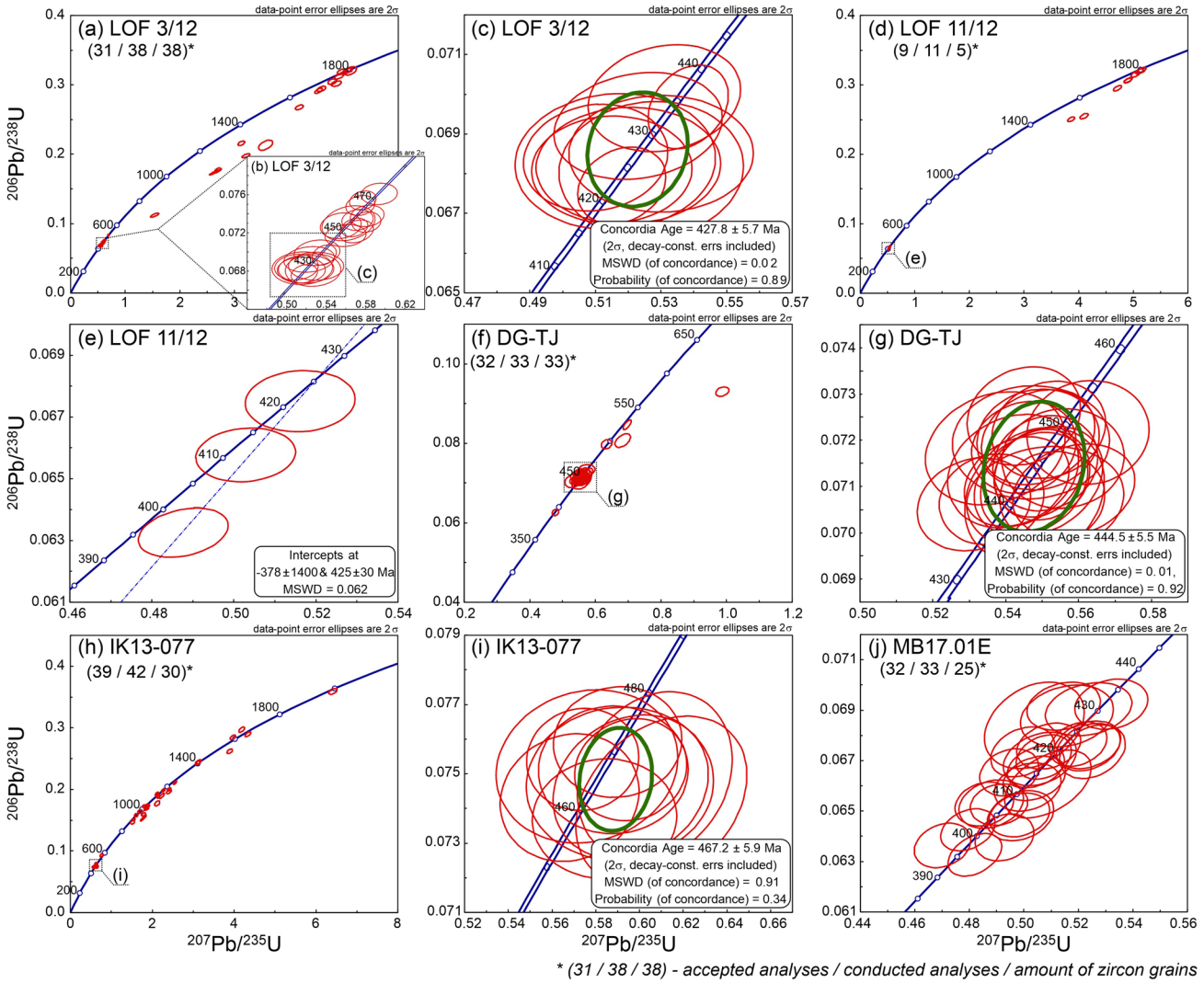

Fig. 6 Concordia plots with results of U–Pb zircon dating

cores, which are dark in CL imaging, and rims with oscillatory, convolute or irregularly-zoned CL bright features which are occasionally homogeneous (Fig. 5d). The cores are characterized by high concentrations of HREE (707.7–2489.8 ppm) with Th/U ratios of 0.22–2.32, and provided $^{206}Pb/^{238}U$ and $^{207}Pb/^{206}Pb$ dates scattered from 920 ± 21 to 1986 ± 18 Ma (n = 25; − 4.2–8.7% disc.; Figs. 6h, 7d, 8d). Temperatures calculated for conditions during the growth of zircon cores range from 693 to 804 °C (5.6–28.0 ppm Ti; Supplementary Table S3.2). The rims show lower concentrations of HREE (48.4–140.9 ppm), Th/U ratios of 0.01–0.04, and low contents of Ti, usually below the detection limit, yielding temperatures of < 614–644 °C. The rims yielded $^{206}Pb/^{238}U$ dates of 458 ± 9 Ma to 492 ± 10 Ma (− 6.9–1.2% disc.), with a Concordia age 467.2 ± 5.9 Ma (n = 13, 2σ, MSWD = 0.91; Fig. 6i).

Blåhø Nappe (Nordøyane Archipelago)

Zircon in eclogite MB17.01E forms subhedral, anhedral to rounded grains with sizes of 50 × 60 to 130 × 200 µm. Twenty-five grains were analyzed with 20 trace element and 28 U–Pb analyses that were accepted for further statistics. Zircon grains show oscillatory or sector zoning, with occasional presence of brighter rims in CL imaging (Fig. 5e). Zircons have low concentrations of HREE (32.0–130.7 ppm) and Th/U ratios ranging from 0.02 to

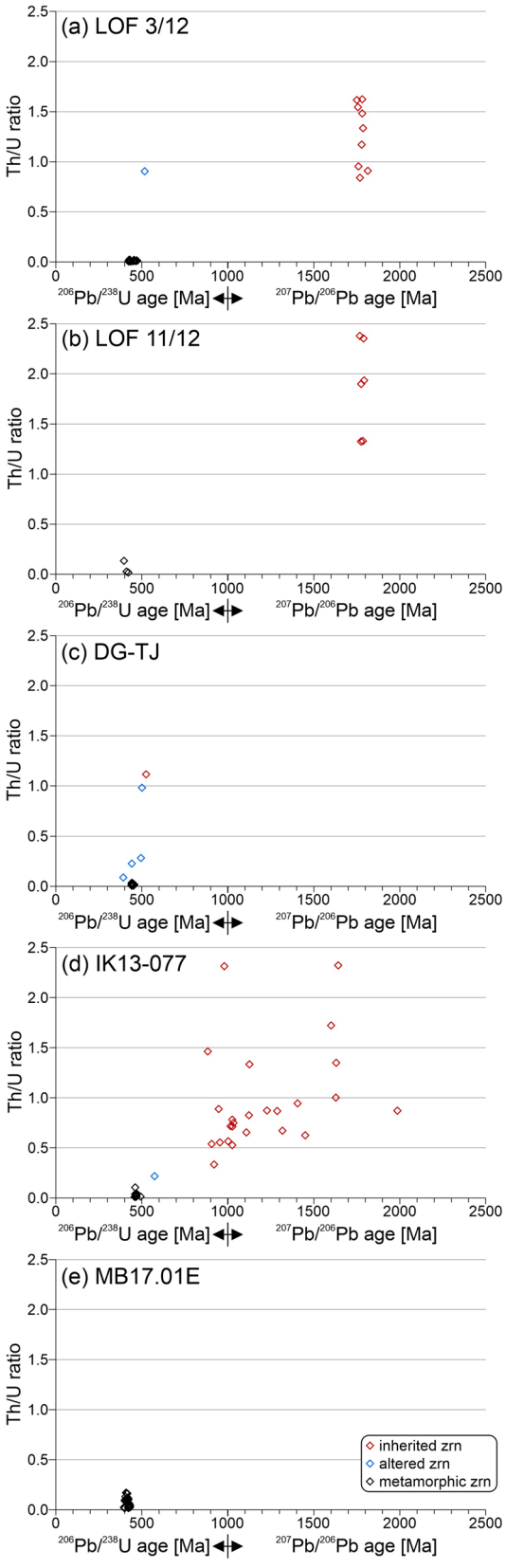

Fig. 7 Diagrams presenting age vs Th/U ratio in zircons. ^{206}Pb/^{238}U and ^{207}Pb/^{206}Pb dates below ± 10% discordance are presented for data < 1000 and > 1000 Ma, respectively

0.17 (Fig. 8e). Twenty-four zircons yielded a cluster of concordant ^{206}Pb/^{238}U dates (− 3.1–1.8% disc.) continuously spread from 395 ± 4 to 430 ± 5 Ma (Figs. 6j, 7e). Calculated Ti-in-zircon temperatures yielded a range of 618 to 765 °C (from < 2 to 12.2 ppm Ti; Supplementary Table S3.2) without visible correlation between temperatures and ages.

Apatite

Lofoten-Vesterålen complex (Lofoten Archipelago)

Apatite in the Lofoten eclogite forms subhedral to anhedral grains with sizes from ca. 50 µm up to several hundred microns in diameter, usually forming intergrowths with garnet, but singular grains can also be found within the matrix (Fig. 9a, b, c). Apatite grains are homogeneous in the BSE images and show limited compositional variations in major elements, i.e., 40.14–42.58 wt.% P_2O_5, and 51.99–56.08 wt.% CaO (Supplementary Table S2.1). The halogen composition of apatites from the Lofoten eclogites is variable between the three main halogen compounds: F, Cl, and OH. For the LOF3/12 eclogite, the fluorapatite component is dominant (0.87 to 1.20 a.p.f.u. F), joined with the chlorapatite component substitution (0.13–0.51 a.p.f.u. Cl), and the hydroxylapatite component (0.31–0.53 a.p.f.u. OH; calculated based on ideal stoichiometry; Ketcham 2015; Fig. 10b; Supplementary Table S2.1). In the case of the LOF11/12 eclogite, apatites have a less significant fluorapatite component (0.10–0.99 a.p.f.u. F), with higher contents of the chlorapatite component (0.20–1.65 a.p.f.u. Cl), as well as higher concentrations of the hydroxylapatite component (0.25–1.18 a.p.f.u. OH; Fig. 10b; Supplementary Table S2.1). Chondrite-normalized REE patterns of Lofoten apatites are generally flat for LREE with positive Eu anomalies (Eu/Eu* up to 3.76; Figs. 8f, g, 10c), followed by a negative slope from Gd to Lu representing depletion in HREE (Fig. 8f, g) with negative Y anomalies (Y/Y* = 0.48–0.81; Fig. 8f, g). Positive Eu anomalies recorded in apatite are similar to positive Eu anomalies in the whole rock composition for these eclogites. Additionally, trace element characteristics of apatites from the Lofoten Archipelago include high Sr/Y ratios of 4.41–275.38 for LOF3/12, and 39.89–2868.17 for LOF11/12, together with high Th/U ratios from 0.70 to 8.67 (Fig. 10d). Apatites from eclogite LOF11/12 have the lowest concentrations of REE (65–1197 ppm) amongst the investigated eclogites, with a strong depletion of HREE with respect to LREE (La/Lu_N ratio 9.73–130.13; Supplementary Table S3.4; Fig. 10e). Eclogite LOF3/12 apatites have the highest concentrations of As out of all samples (average 176 ppm, Supplementary Table S3.4). LA-ICPMS U–Pb dating of apatite from Lofoten eclogites yielded lower

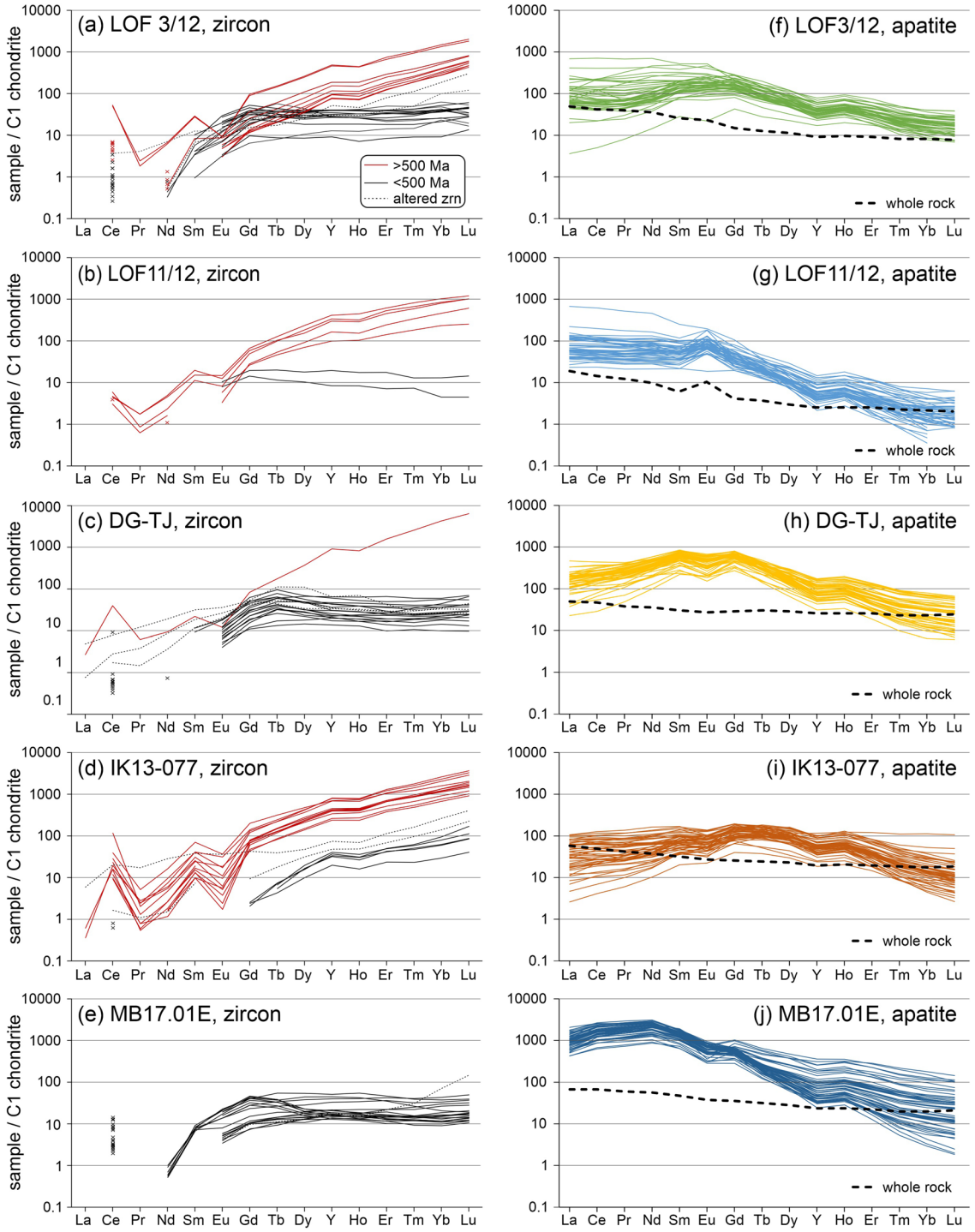

Fig. 8 Chondrite normalized plots for **a**–**e** zircon, **f**–**j** apatite and whole rock data. Chondrite normalizing values are taken from McDonough and Sun (1995)

intercept ages of 322 ± 28 Ma (LOF3/12) and 354 ± 33 Ma (LOF11/12; Fig. 11a, b). Six U–Pb analyses of apatites from eclogite LOF11/12 plot along a separate trend in Concordia space suggesting the presence of a younger population with a lower intercept age 227 ± 24 Ma (Fig. 11c).

Lower Seve Nappe (Northern Jämtland)

Apatites from the two LSN eclogites (DG-TJ and IK13-077) form subhedral to anhedral grains in the rock matrix that are homogeneous in BSE imaging, differing in size from a few

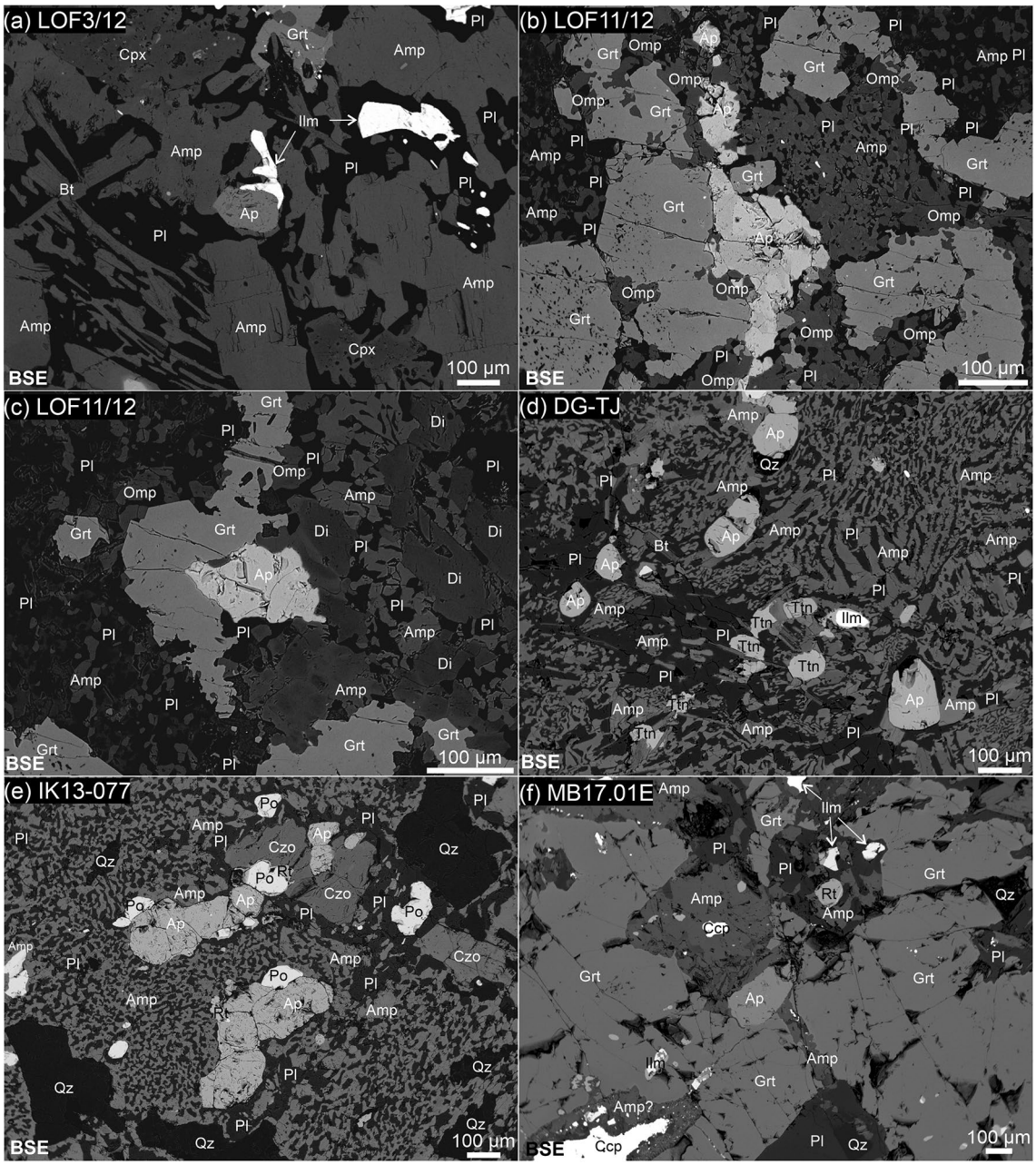

Fig. 9 BSE images of microtextures containing the apatite in eclogite samples. *Amp* amphibole, *Ap* apatite, *Bt* biotite, *Ccp* chalcopyrite, *Czo* clinozoisite, *Di* diopsite, *Grt* garnet, *Ilm* ilmenite, *Pl* plagioclase, *Po* pyrrhotite, *Omp* omphacite, *Rt* rutile, *Ttn* titanite, *Qz* quartz

dozen to a few hundred micrometers in diameter (Fig. 9d, e). The major cations do not show strong variations between the two samples with 41.32–43.41 wt.% P_2O_5 and 52.69–56.86 wt.% CaO (Supplementary Table S2.1). Regarding the halogen composition, apatites in both eclogites have minor chlorapatite components (0.00–0.10 a.p.f.u. Cl). Fluorapatite is the dominant type of apatite in eclogite DG-TJ (1.05–1.49 a.p.f.u. F) with a subordinate hydroxylapatite component (0.50–0.95 a.p.f.u. OH). In contrast, apatites in eclogite IK13-077 have more significant hydroxylapatite component concentrations in relation to the fluorapatite component (0.83–1.06 a.p.f.u. OH and 0.89–1.14 a.p.f.u. F; Fig. 10b, Supplementary Table S2.1). The two eclogites from the LSN also yield different apatite trace element characteristics and U–Pb dating results. The main differences in the REE concentrations include higher REE content in apatite from eclogite DG-TJ compared to IK13-077, i.e., 420–1207 ppm vs. 63–372 ppm, respectively (Fig. 10a, c, e, f, Supplementary Table S3.4). Apatites from both eclogites show bell-shaped chondrite-normalized patterns, with

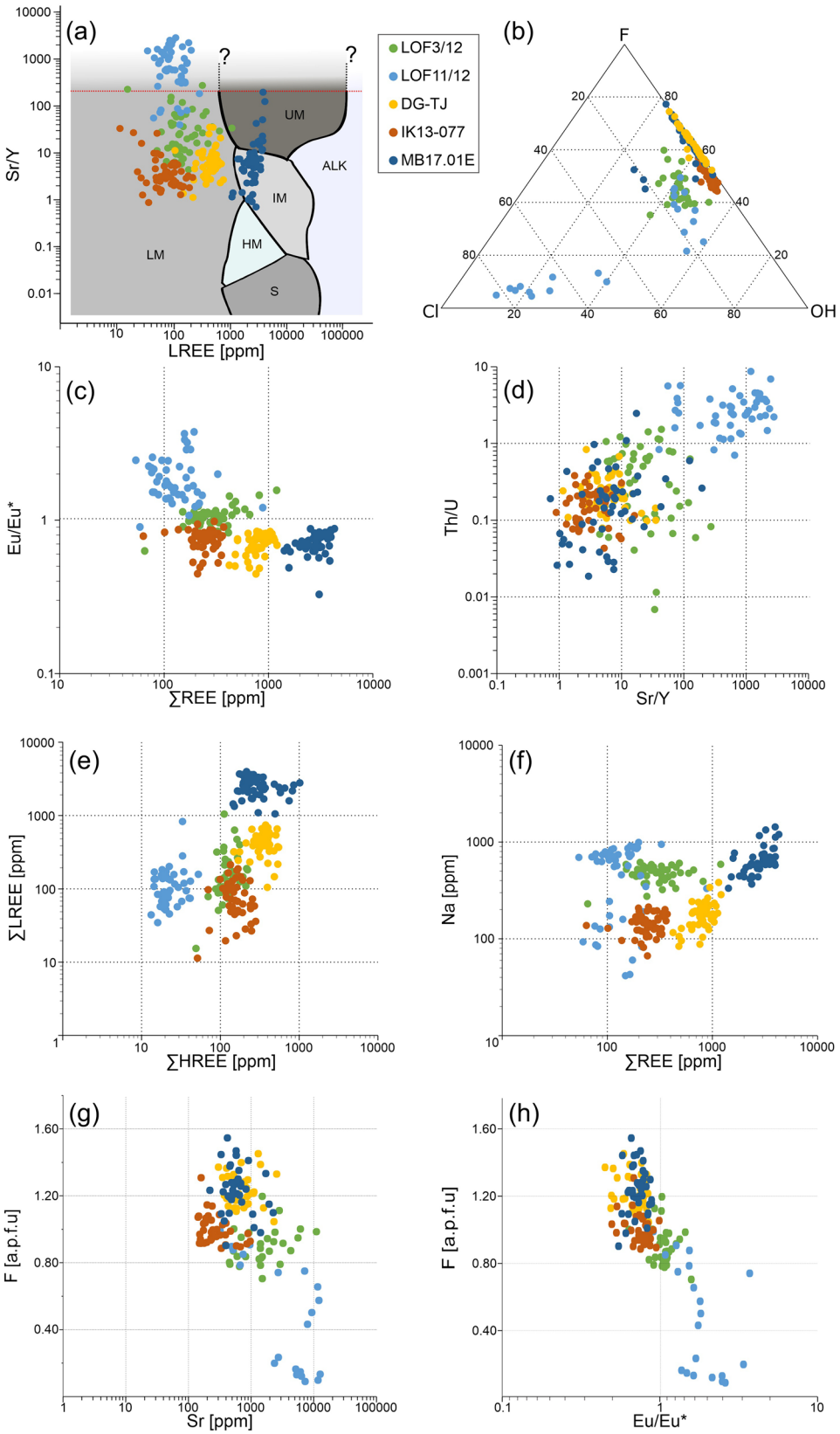

Fig. 10 Diagrams presenting detailed trace element and volatile composition of apatite. **a** LREE vs. Sr/Y plot against the SVM classification diagram of O'Sullivan et al. (2020); dotted red line marks the end of fields defined by the initial database above which continuation of the fields is extrapolated for the purpose of the figure (abbreviations for groups: ALK = alkali-rich igneous rocks; IM = mafic I-type granitoids and mafic igneous rocks; LM = low- and medium-grade metamorphic and metasomatic; HM = partial-melts/leucosomes/high-grade metamorphic; S = S-type granitoids and high aluminium saturation index (ASI) 'felsic' I-types; UM = ultramafic rocks including carbonatites, lherzolites and pyroxenites). **b** Triangular plot of halogen composition of studied apatites based on the EPMA measurements (OH contents calculated based on the ideal stoichiometry of apatite X position). **c** Sums of REE vs. values of Eu anomalies. **d** Sr/Y ratios vs. Th/U ratios. **e** Sums of HREE vs. sums of LREE. **f** Sum of REE vs. content of Na in apatite. **g** Concentration of Sr vs. calculated F content. **h** Values of Eu anomalies vs. calculated F contents

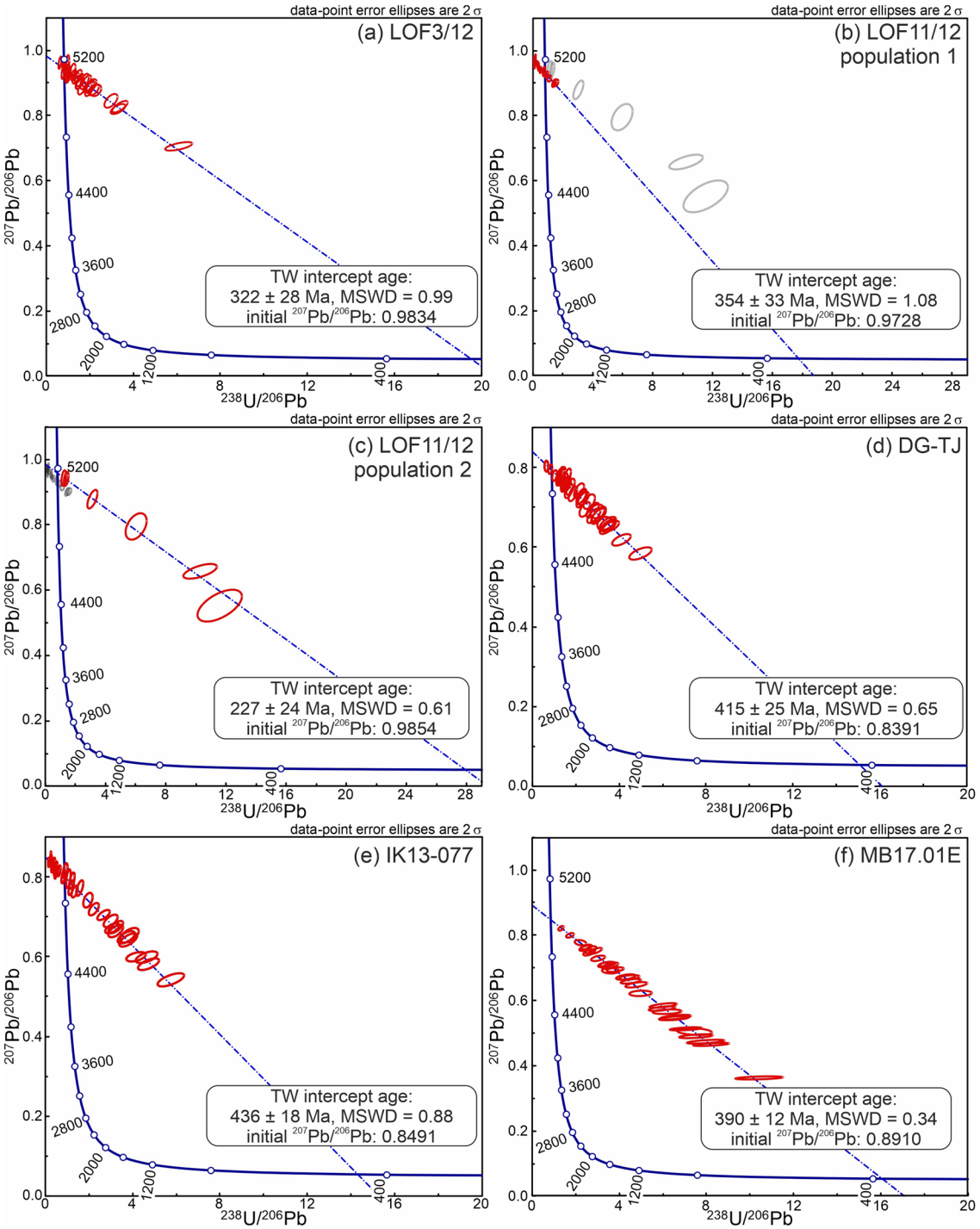

Fig. 11 Concordia plots with results of U–Pb apatite dating

average $La/Sm_N = 0.30$ and 0.55 and $La/Lu_N = 9.33$ and 5.50, in eclogites DG-TJ and IK13-077, respectively. The Eu anomalies for both samples are negative (average Eu/Eu* = 0.73; Figs. 8h, i, 10c, h; Supplementary Table S3.4). LA-ICPMS U–Pb analyses of apatites yielded two different lower intercepts ages, with 415 ± 25 Ma (MSWD = 0.65) for eclogite DG-TJ, and 436 ± 18 Ma (MSWD = 0.88) for eclogite IK13-077 (Fig. 11d, e).

Blåhø Nappe (Nordøyane Archipelago)

Apatites in the Blåhø Nappe eclogite (MB17.01E) form subhedral to anhedral grains ca. 100 × 200 µm in size (Fig. 9f). BSE imaging of separated apatite grains revealed the presence of linearly oriented, micro- to nanoinclusions (ca. < 2 µm in diameter) of chalcopyrite within otherwise homogenous grains. The main cation compositions in the apatites are consistent with 41.20–43.12 wt.% P_2O_5 and 53.91–56.25 wt.% CaO (Supplementary Table S2.1). Fluorapatite is the dominant endmember in the apatite (1.01–1.55 a.p.f.u. F), which usually also have low content of chlorapatite (0.00–0.03 a.p.f.u. Cl). However, there are a few analyses that record higher concentrations of Cl (0.06–0.43 a.p.f.u.). The hydroxylapatite component comprises the rest of the anion composition, assuming ideal stoichiometry (0.45–0.98 a.p.f.u. OH; Fig. 10b, Supplementary Table S2.1). Apatites from the Blåhø Nappe eclogite recorded the highest concentrations of REE (1418–4284 ppm) among the studied eclogites, especially with visible enrichment in LREE (957–3749 ppm), exhibiting a decline towards HREE in the chondrite-normalized pattern (average $La/Lu_N = 110.67$; Figs. 8j, 10c, e, f; Supplementary Table S3.4). Apatites from eclogite MB17.01E also have the highest concentrations of Na (333–1433 ppm), U (4.61–51.62 ppm), and Th (0.56–18.09 ppm), together with elevated amounts of Fe in the structure (271–1068 ppm). The U–Pb dating of apatites, based on analyses of 30 grains, provided a lower intercept age of 390 ± 12 Ma (MSWD = 0.34, Fig. 11f).

Discussion

Inherited zircon—records of events prior to subduction and metamorphism

Out of the whole set of samples, inherited zircon grains were present in both eclogites from LVC (LOF3/12 and LOF11/12) and also in one of the samples from the LSN (IK13-077). The inherited zircon domains are usually found as the cores of composite grains that are dark in CL images and commonly exhibit irregular boundaries with CL-bright rims. The presence of oscillatory growth zoning, high HREE contents and Th/U ratios well above 0.4 (Figs. 5a, b, d, 7a, b, d, 8a, b, d) indicates the igneous origin of zircon (cf., Hoskin and Black 2000; Kelly and Harley 2005; Rubatto 2017). In the Lofoten eclogites, the age cluster at ca. 1800 Ma from the inherited zircon domains is consistent with earlier geochronology of the crystalline basement rocks of the LVC (Corfu 2004a; Fig. 7a, b). All the U–Pb data from the inherited domains plot along a discordia line with upper and lower intercepts at ca. 1800 Ma and ca. 420–440 Ma, respectively, indicating that a relic component of the Paleoproterozoic mafic protolith metamorphosed under eclogite-facies conditions during Caledonian metamorphism (Fig. 6a–e; Markl and Bucher 1997). In case of the LSN eclogite, U–Pb dating of inherited zircon domains resulted in scattered dates ranging from 883 to 1986 Ma with cluster of ages around 1000 Ma (Fig. 7d). These ages correlate well with the U–Pb ages of detrital zircon from the metasediments of Middle Allochthon within Seve Nappe Complex (Gee et al. 2014, 2015). This suggests that the mafic protolith was supplied with zircons derived from the surrounding sedimentary rocks, followed by later (U)HP metamorphism during subduction.

Metamorphic zircon—isotopic and trace element records of metamorphism

Metamorphic zircon domains in all samples exhibit varying levels of brightness in CL images, either forming rims on the relic cores or are found as whole grains that vary in texture from homogenous to heterogeneous with different zoning patterns (Fig. 5). The contrast with the inherited zircon is easily recognized when both domains are present, with metamorphic domains being much brighter, common for metamorphic zircon (cf., Rubatto 2002, 2017; Corfu et al. 2003a, b; Whitehouse and Platt 2003; Bingen et al. 2004; Chen et al. 2010). The two textural types of metamorphic zircon share similar trends in trace element characteristics, such as low concentrations of HREE compared to the inherited domains (Fig. 8a–e). The variable Th/U ratios of 0.00–0.17 and U–Pb ages in range of 467.2 Ma to 395.4 Ma (Figs. 6, 7) indicate various records of Caledonian metamorphism for different eclogites.

In case of the zircons from the LVC eclogites, depletion in HREE, manifesting in flat chondrite normalized patterns ($Lu_n/Gd_n < 3$; Fig. 8a, b), indicate that zircon grew in the presence of garnet (cf., Rubatto 2002; Harley et al. 2007; Rubatto and Hermann 2007). Additionally, a weak negative Eu anomaly in chondrite normalized plots ($Eu/Eu^* > 0.75$; Fig. 8a, b) suggests zircon growth in plagioclase-unstable conditions at high pressures (Rubatto and Hermann 2007). Earlier Lu–Hf dating of garnet resolved the age of eclogite-facies metamorphism to 399 ± 10 Ma (Froitzheim et al. 2016). The $^{206}Pb/^{238}U$ dating of zircon in this study provided two populations of Early Paleozoic ages, an older one spanning from 475 to 450 Ma and a younger one with a Concordia age of 427.8 ± 5.7 Ma (n = 10, 2σ, MSWD = 0.02; Fig. 6b, c). The older population correlates with the amphibolite facies metamorphic events recorded between 469 and 461 Ma in the Lofoten area (Corfu 2004a; Steltenpohl et al. 2011a, b; Froitzheim et al. 2016). The 427.8 ± 5.7 Ma zircon population, which records garnet growth, does not match the previous Lu–Hf garnet age of 399 ± 10 Ma from eclogite at

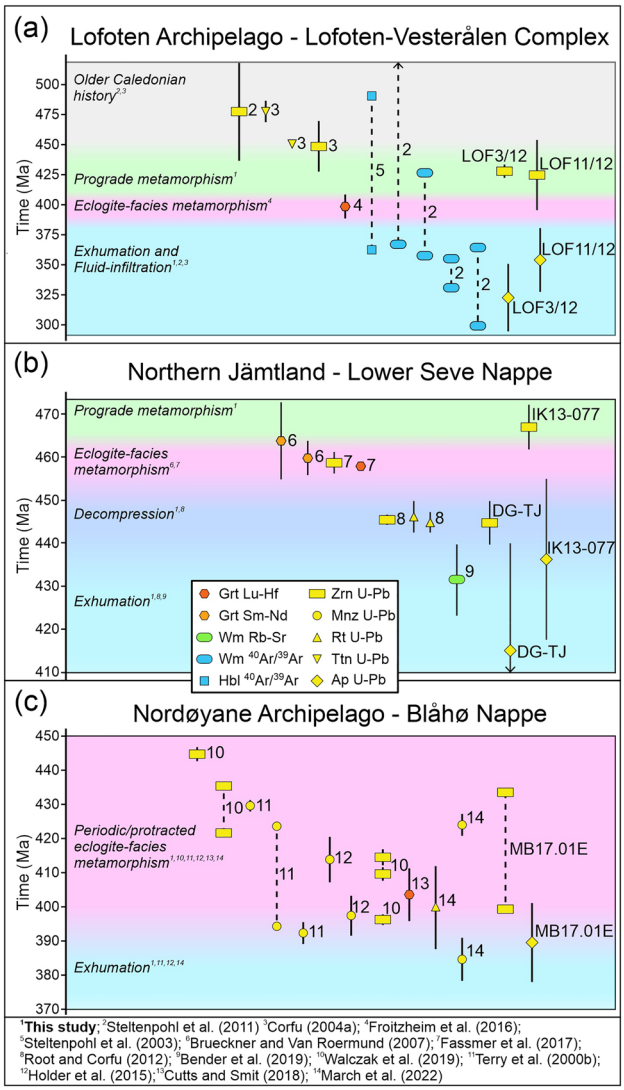

Fig. 12 Summary of the geochronological data for each of the studied complexes, presenting data from this study and earlier works. Error bars are given with 2σ confidence level. [1] This study; [2] Steltenpohl et al. (2011a, b) [3] Corfu (2004a); [4] Froitzheim et al. (2016); [5] Steltenpohl et al. (2003); [6] Brueckner and Van Roermund (2007); [7] Fassmer et al. (2017); [8] Root and Corfu (2012); [9] Bender et al. (2019); [10] Walczak et al. (2019); [11] Terry et al. (2000b); [12] Holder et al. (2015); [13] Cutts and Smit (2018); [14] March et al. (2022)

the same mafic exposure (Fig. 12a; Froitzheim et al. 2016). Diffusional resetting of the Lu–Hf system in garnet is not predicted as temperatures did not exceed ~ 650 °C (Froitzheim et al. 2016; Bloch et al. 2020). Thus, it is possible that the zircon may record an earlier stage of HP metamorphism and an older generation of garnet growth, progressing to UHP metamorphism at 399 ± 10 Ma. It is also possible that the differences between these age records could reflect two separate events of HP metamorphism, first at ca. 425 Ma (this study) and second at ca. 399 Ma (Froitzheim et al. 2016) in the subduction-exhumation cycles following the dunk tectonics model for the Scandinavian Caledonides (Fig. 12a; Brueckner et al. 2004; Brueckner 2006; Majka et al. 2014). Both scenario span the evolution of the Baltica-Laurentia collision (425–400 Ma; Kylander-Clark et al. 2009).

The two eclogite samples collected from the LSN show different geochemical and geochronological characteristics of zircon (Figs. 6f–i, 7c, d, 8c, d). In the case of sample IK13-077, the zircon grains have well defined core and rim textures, with inherited Proterozoic cores that occur to a much lesser extent in sample DG-TJ (Fig. 5c, d). This was most likely caused by the variability in the composition of the initial rocks that were subducted. Even though the metamorphic domains have HREE concentrations significantly lower than the inherited cores, they have the same REE slope in the chondrite normalized plots (Fig. 8d) with ratios of Lu_n/Gd_n from 17.4 to 70.8, suggesting that growth of the metamorphic zircon preceded garnet (Rubatto 2002; Harley et al. 2007; Rubatto and Hermann 2007). This interpretation is in agreement with the $^{206}Pb/^{238}U$ age of 467.2 ± 5.9 Ma being older than previous results of Sm–Nd and Lu–Hf garnet dating of ca. 458 Ma for the samples from LSN (Brueckner and Van Roermund 2007; Fassmer et al. 2017; Figs. 2b, 6i). Therefore, the 467.2 ± 5.9 Ma age is interpreted as the growth of the metamorphic zircon during prograde stages of subduction of the LSN before garnet growth (Fig. 12b).

Zircons from eclogite DG-TJ, in contrast to those from the eclogite IK13-077, are almost completely composed of metamorphic domains. Only a single analysis of a grain core yielded higher concentrations of HREE and Th/U ratios, similar to other inherited zircon cores in this paper. However, the U–Pb date obtained within this grain was significantly lower at 524 ± 6 Ma, suggesting that it is possibly an inherited grain overprinted by metamorphism. The concordia age of 444.5 ± 5.5 Ma for the metamorphic zircon from eclogite DG-TJ (Fig. 6g) is consistent with earlier 446.3 ± 3.7 Ma and 445.2 ± 2.1 Ma U–Pb ages of zircon and rutile, respectively (Root and Corfu 2012). These ages collectively contrast the older Sm–Nd and Lu–Hf garnet ages of ca. 458 Ma from the Tjeliken eclogites (Brueckner and van Roermund 2007; Fassmer et al. 2017; Figs. 2b, 6g). Chondrite normalized plots of the DG-TJ metamorphic zircon show flat HREE patterns with Lu_n/Gd_n ratios < 3, suggesting zircon grew coeval with or subsequent to garnet (Rubatto 2002; Harley et al. 2007; Rubatto and Hermann 2007). Textural evidence shows that at least some zircon growth was supplied with Zr by rutile partially replaced by ilmenite and titanite (Fig. 4a, b), typically linked with retrogressive metamorphism during decompression (Kohn et al. 2015). The calculated Ti-in-zircon temperatures of 620–698 °C, representing conditions of the zircon growth, are high

enough to exceed the closure temperature for Pb diffusion in rutile (570–630 °C), which is in agreement with rutile recording isotopic closure at ca. 445 Ma during exhumation and cooling of the rocks (Cherniak 2000; Kooijman et al. 2010). This explains the correlations between the U–Pb ages of zircon and rutile that are younger than garnet crystallization (Brueckner and van Roermund 2007; Root and Corfu 2012; Fassmer et al. 2017). Therefore, the U–Pb age of 444.5 ± 5.5 Ma corroborates the previous postulation that zircon grew coevally with breakdown of rutile during the retrograde metamorphism during exhumation (Fassmer et al. 2017; Fig. 12b).

Zircon grains in eclogite MB17.01E all feature bright domains in CL images with sector or patchy zoning and a lack of distinct inherited core—metamorphic rim textures (Fig. 5e). The flat HREE patterns of metamorphic zircon in the chondrite-normalized plot ($Lu_n/Gd_n < 3$; Fig. 8e) suggest that zircon grew either coeval with or subsequent to garnet (Rubatto 2002; Harley et al. 2007; Rubatto and Hermann 2007). Similar to the eclogite DG-TJ, microtextural features suggest that some zircon could have formed due to rutile breakdown (Fig. 4c, d). The Lu–Hf garnet date of 404.5 ± 7.9 Ma from the Nordøyane eclogite (Cutts and Smit 2018) suggests the age of garnet re-equilibration after multiple HP-HT metamorphic events. The low precision of the Lu–Hf age was attributed to high Lu/Hf ratios and homogenized composition of garnet (Cutts and Smit 2018; see sample 14-06-FJ). Recent zircon and rutile U–Pb geochronology of gneisses that accompany eclogites on Fjørtoft island provided a collection of concordant Caledonian dates ranging from ca. 450 Ma to ca. 378 Ma, suggesting either a protracted period of zircon recrystallization and Pb-loss, or multiple discrete zircon-forming metamorphic events (Walczak et al. 2019; March et al. 2022). Two distinct high-grade metamorphic events in the tectonic evolution of this area were proposed. The first event has been constrained to 446.2 ± 2.1 Ma, whereas the second includes multiple events from ca. 437 to ca. 423 Ma, with scattered younger dates of ca. 417–397 Ma related to the retrograde metamorphism (Walczak et al. 2019). Additionally, monazite U–Pb geochronology provided two populations of Caledonian ages, one clustered around 423 Ma and interpreted as the possible age of early stages of (U)HP metamorphism, and the second population at ca. 385 Ma that could be related to cooling in the region (March et al. 2022).

Our U–Pb zircon data for the Fjørtoft eclogite, forming a continuous span of dates from ca. 430 to 395 Ma, reproduce previous geochronological patterns from gneisses in the area. The lack of any clusters within the specific ages suggest that the previously distinguished second metamorphic event is more likely a part of a longer process including several cycles of (U)HP-HT metamorphism within short intervals from each other occurring at the final stages of the Scandian collision and transitioning smoothly into retrogression metamorphism related to exhumation. In such case, it is difficult to resolve those cycles with the resolution of the zircon U–Pb dating in the eclogite MB17.01E. The continuous concordant cluster of dates indicates prolonged zircon growth from 430 to 395 Ma, which could also be a result of partial overprint due to thermal event(s) postdating zircon growth.

Trace element characteristic of apatite in eclogites

The results of BSE imaging and EPMA-WDS analysis demonstrate that apatites from all studied eclogites have similar major element content and no chemical zoning is apparent. However, significant variations exist in trace element and halogen content (Fig. 10). In particular, both the absolute REE content and the REE patterns for apatites vary between the eclogite samples. The absolute apatite REE content is positively correlated with bulk rock REE content, suggesting the former is a function of the latter. The most common substitution mechanisms that allow incorporation of REE into the apatite structure include $2REE^{3+} \rightarrow 3Ca^{2+}$; $REE^{3+} + Na^{+} \rightarrow 2Ca^{2+}$; $REE^{3+} + SiO_4^{4-} \rightarrow Ca^{2+} + PO_4^{3}$ (Fleet and Pan 1995; Pan and Fleet 2002). Because samples DG-TJ, MB17.01E and, to a lesser degree, IK13-077, all show linear positive correlations between Na vs. REE (Fig. 10f), the $REE^{3+} + Na^{+} \rightarrow 2Ca^{2+}$ substitution seems to be the predominant among the studied apatites.

In contrast to the correlation of absolute REE content between apatite and bulk rock, the apatite REE trends generally do not match the bulk rock REE trends, with the exception of the positive Eu anomaly from apatite in eclogite LOF11/12. The dissociated REE patterns indicate that apatites also provide distinct records of metamorphic processes in the eclogite (Fig. 8f–j). All apatites share the general trend of negative HREE slopes with negative Y-anomalies in the chondrite-normalized plots with respect to the bulk rock. These patterns can be attributed to the incorporation of HREE and Y into garnet, which is an abundant phase in the eclogites, and possibly, to a lesser extent, into zircon (cf. Grauch 1989). The apatite LREE patterns also do not follow the bulk rock REE trends. Apatites in all samples show flat to positively inclined LREE patterns, with distinctly elevated LREE pattern of MB17.01E apatites (Figs. 8f–j, 10a, e). The data prevent drawing far-reaching conclusions, nevertheless, these patterns are partially explained by coeval or subsequent growth of apatites with phases preferentially incorporating LREE, such as epidote in DG-TJ eclogite (Fig. 4b; cf. Gieré and Sorensen 2004; Henrichs et al. 2018, 2019; Jepson et al. 2021) or monazite, which has been reported in eclogites from the studied regions (Terry et al. 2000b; Holder et al. 2015; March et al. 2022).

High concentrations of Sr are recorded by all apatites investigated here, with extremely high Sr concentrations in apatites from Lofoten region, replicating the bulk composition of the Lofoten eclogite samples (Fig. 10a; Supplementary Table S4). The high Sr contents and lack of distinct negative Eu anomaly in chondrite-normalized patterns of apatites generally suggest the absence of plagioclase during their growth in the investigated eclogites (Figs. 8f–j, 10a, c). The LREE, Th, and U enrichment in apatites from high-grade metamorphic processes can be the result of titanite and/or allanite breakdown during prograde metamorphism, together with solid state diffusion during prolonged time spent in HT conditions (Bingen et al. 1996; Cherniak 2010; Henrichs et al. 2018, 2019; O'Sullivan et al. 2020). Apatite could have been stabilized by F supplied by biotite breakdown, thus becoming a sink for LREE, Th, and U in the eclogite (cf., Bingen et al. 1996; Jepson et al. 2021). In that sense, the apatite could have crystalized coevally with zircon and/or garnet, but at the high temperature conditions it behaved as an open system until cooling below ~ 550 °C (Bingen et al. 1996; Chew and Spikings 2015; Jepson et al. 2021). Therefore, characteristics of LREE and HREE patterns, presence / absence of Y and Eu anomalies, as well as characteristics of Sr concentrations, fingerprint metamorphic processes recorded by apatites, indicating formation during the HP history of the eclogites.

Apatite as a fingerprint of metasomatic processes

Fluorapatite is the dominant type in most of metamorphic and magmatic rocks due to preferential partitioning of F into the apatite structure with varying additions of OH or Cl, depending on the conditions of apatite growth and/or alteration processes (Zhu and Sverjensky 1991; Sha and Chappell 1999; Pan and Fleet 2002; Piccoli and Candela 2002; Spear and Pyle 2002; Schettler et al. 2011; Harlov 2015). Among studied eclogites, apatite halogen compositions show dispersion with varying concentrations of F, Cl and OH within the same sample. The dispersion of halogens could suggest interactions with fluids since halogens in apatite are very sensitive to such changes and can easily exchange with the fluid not necessarily affecting the overall composition of apatite.

In case of both LVC samples, apatites contain high amount of Cl, including a few analyses in LOF11/12 sample where Cl is the main halogen component (Fig. 10b, Supplementary Table S2.1). Presence of Cl-rich phases (e.g., amphibolite, biotite, scapolite) is one of the known features of metamorphic rocks in the Lofoten region (Kullerud 1992, 1995, 1996; Kullerud and Erambert 1999). Therefore, we interpret the Cl-rich component of apatite to be inherited from the eclogite protolith or fluids responsible for eclogitization of the protolith, whereas later-stage fluid induced dissolution-reprecipitation processes resulted in the exchange of Cl with more preferential F and OH (cf. Harlov and Förster 2003; Krause et al. 2013). Re-equilibration of halogens may also be reflected in trace element dispersions as indicated by decreasing Sr and Eu contents in apatite grains with lower Cl concentrations and consequently higher concentrations of F (Fig. 10g, h; Supplementary Tables S2.1, S3.4). This also explains the lower concentrations of REE recorded in Lofoten samples and the lack of correlation between Si, Na and REE (Fig. 10f).

In the apatites from eclogite DG-TJ from the LSN, the dominant end-member is fluorapatite with slightly varying OH components and negligible contents of Cl. Despite disperse halogen composition there are no clear indications of potential metasomatic alteration in trace element of apatites in this sample (Fig. 10b; Supplementary Table S2.1). The relatively uniform, bell-shaped chondrite-normalized REE patterns with well-defined Y and Eu negative anomalies show the consistent chemistry of apatites during the evolution of the Tjeliken eclogite (Fig. 8h). If the dispersion of F and OH in apatites from DG-TJ eclogite indicates interactions with the fluids, the trace element would not have responded to this interaction and remained robust records of crystallization.

The apatites from eclogite IK13-077 differ from the DG-TJ sample regarding halogen composition where OH component is more pronounced with some trace amounts of Cl also present (Fig. 10b; Supplementary Table S2.1). Additionally, there is a correlation between halogen discrepancies and the trace element characteristics of apatites with Sr concentrations decreasing and Eu/Eu* negative anomalies getting more pronounced with increasing F content in apatites (Fig. 10g, h). The REE in IK13-077 apatites have lower concentrations compared to DG-TJ and are more variable with dispersed chondrite-normalized patterns for LREE and HREE (Fig. 8i; Supplementary Table S3.4). Additionally, the less clear correlation between Si or Na vs. REE, shifted similarly to the LVC samples, could possibly reflect post-crystallization alteration processes, which might be responsible for partial removal of REE (particularly LREE) from the structure due to fluid-induced alterations during retrogression (Fig. 12b; cf., Harlov and Förster 2003; Krause et al. 2013).

The halogen composition of the MB17.01E eclogite from the Blåhø Nappe is similar to the samples from LSN described above with the dominant substitution of fluorapatite with a lesser contribution of the OH component and uncommon increase of Cl contents (Fig. 10b). The dispersion of the halogen composition in this sample could indicate apatite growth during a dynamically changing environment over an extended period of time (i.e., multiple metamorphic events with different fluid compositions), or heterogeneous

metasomatism of the apatite after crystallization. The compositional trace element characteristics of apatites from MB17.01E eclogite generally contrast those of apatites from the other regions with elevated concentrations of LREE as well as U and Th. The chondrite-normalized REE patterns are uniform in the LREE region, whereas towards the HREE they become more scattered (Fig. 8j). Enrichment in the LREE indicates lack of other LREE-bearing phases during apatite growth whereas scattered HREE content is attributed to the influence of the behaviour of garnet and zircon. To conclude, the preserved linear trend of Na vs. REE, high amounts of LREE and U, slight dispersion of the Eu anomaly, negative Y anomaly and the negative slope of HREE chondrite-normalized patterns indicate that apatite crystallized in HP conditions in the presence of garnet and absence of plagioclase, followed by metasomatism in the presence of plagioclase and partial consumption of garnet that released HREE + Y. The lack of LREE dispersion may reflect that no LREE-bearing phase grew during the fluid-alteration event of apatite, therefore, no LREE was sequestered from apatite.

Apatite geochronology

The trace element records of apatites generally indicate they formed as part of the HP eclogite mineral assemblage in the presence of garnet and absence of plagioclase. Formation of apatite in HP conditions necessitates that it formed in temperature conditions exceeding the apatite Pb closure temperature, based on previous P–T studies of the three regions (Dobrzhinetskaya 1995; Majka et al. 2014; Froitzheim et al. 2016; Fassmer et al. 2017; Gilio et al. 2021). Thus, apatites either record cooling or Pb loss due to metasomatism (e.g., dissolution-reprecipitation reactions).

For the LVC eclogites, the U–Pb apatite data include two age populations (1) 354 ± 33 and 322 ± 28 Ma ages staying within their uncertainties, and (2) 227 ± 24 Ma (Fig. 11a–c), all considerably younger than the U–Pb zircon ages from the LVC eclogites. The age discrepancy between zircon and apatite in each sample is interpreted to be related to volume diffusion of Pb, which occurs through the apatite structure in temperature conditions above ca. 350–550 °C (Cherniak 2010; Chew et al. 2011; Chew and Spikings 2015). Consequently, with regard to the trace element and halogen composition of apatites from Lofoten samples, the ages of 354–322 Ma are interpreted to provide the timing of the retrogressive metamorphism and metasomatic alteration during exhumation of the eclogites. The age is consistent with earlier $^{40}Ar/^{39}Ar$ geochronology of micas that suggested retrogression during the relatively broad timespan of 364–300 Ma (Fig. 12a; Steltenpohl et al. 2011a, b; Fournier et al. 2019). The age of 227 ± 24 Ma in eclogite LOF11/12 suggests a younger overprint involving another reheating episode(s) potentially associated with fluids that affected the U–Pb system in apatite, possibly due to extensional tectonics related to the Pangea break-up and formation of local sedimentary basins (e.g., Steltenpohl et al. 2004, 2011a, b; Fournier et al. 2014).

The different compositional characteristics of apatites from the LSN suggest that apatite resolves different stages and processes during exhumation of the LSN. The slightly older apatite age suggests cooling during exhumation of the IK13-077 eclogite at 436 ± 18 Ma, possibly accompanied by fluid alterations related to the active shear zones as suggested by dispersions in its trace element content. In contrast, the apatite data from eclogite DG-TJ do not show strong evidence for fluid-induced alteration and are interpreted to record cooling of the eclogite at 415 ± 25 Ma below 500–350 °C. It is possible that the two ages may record the same event considering the high uncertainty of the results, however, it cannot be excluded that two distinct events are recorded. This possibility supports the previously proposed idea that the Tjeliken eclogite, together with its host gneiss, may not be a part of LSN, but is rather a klippe of the Middle Seve Nappe (Strömberg et al. 1984; Majka et al. 2014; Klonowska et al. 2016). In such case, apatites from eclogite IK13-077 would represent exhumation of the LSN along its basal shear zone with apatites from DG-TJ recording subsequent activation (or prolongation) of the MSN-LSN shear zone, exhuming the MSN rocks (including Tjeliken). Thus, the potential discrepancy of the apatite U–Pb dates between the two eclogites supports out-of-sequence thrusting of the SNC in northern Jamtland, with distinct events occurring at ca. 430 Ma and ca. 415 Ma (Bender et al. 2018; 2019).

For the Blåhø nappe eclogite, the apatite lower intercept age of 390 ± 12 Ma constrains the age of cooling through 500–350 °C. The HREE, Eu and Y characteristics discussed earlier suggest record of post-crystallization alteration, however, the U–Pb systematics are uniform, indicating record of a single event (Fig. 11). This can be explained by the slower diffusion of REE compared to diffusion of Pb in apatites (Cherniak et al. 1991; Cherniak 2000), with metasomatism occurring in temperature conditions below REE closure, but above Pb closure. As a result, metasomatic patterns recorded by REE may not correlate with their U–Pb record, unlike for zircon. The age of apatite corresponds well to earlier constraints on the cooling ages in the region (Krogh et al. 2011; Walsh et al. 2013; Kylander-Clark and Hacker 2014). Altogether, the apatites in the LSN demonstrate older exhumation ages compared to those in the LVC and in the Blåhø nappe, suggesting earlier exhumation of (U)HP rocks found in the tectono-stratigraphically higher Seve Nappe Complex compared to those in the parautochthonous Baltican basement.

Conclusions

Comprehensive geochronological and geochemical investigations of zircon and apatite from eclogites provide new data that significantly contribute to tectono-metamorphic reconstructions in three regions of the Scandinavian Caledonides. The HREE characteristics, combined with internal textural features, reveal both igneous and metamorphic origins of zircon. They also allow for constraining the stages of growth along the metamorphic P–T path with respect to other HREE- and Zr-bearing phases. The zircon geochronology resolves the timing of prograde metamorphism in the eclogites from the Lofoten-Vesterålen complex at 427.8 ± 5.7 Ma, and in one eclogite from the LSN at 467.2 ± 5.9 Ma. The zircon age representing retrograde metamorphism at 444.5 ± 5.5 Ma is constrained in the second eclogite from the LSN eclogite from Tjeliken Mt. In contrast, protracted high-grade metamorphic event(s) are recorded in the Blåhø Nappe eclogite from ca. 430 to 395 Ma. The new geochronological data complete the earlier zircon geochronology for future tectono-metamorphic reconstructions of the Scandinavian orogen.

The apatite U–Pb data provide new important information constraining timing of the late stages of retrograde metamorphism and exhumation, previously not sufficiently determined in the Scandinavian Caledonides. For the LVC eclogite, apatite U–Pb ages of 354–322 Ma represent the retrogressive metamorphic stage and the metasomatic alterations during exhumation. The ages of 436 ± 18 Ma and 415 ± 25 Ma yielded by apatites from the LSN eclogites correspond to previously determined exhumation stages of the LSN, with apatite recording fluid alterations in one of the studied eclogites, whereas apatite in the second eclogite does not bear signs of alteration. The 390 ± 12 Ma age of apatites from the Blåhø Nappe eclogite resolve cooling of the eclogite after periodic or prolonged (U)HP-HT metamorphism.

In summary, this work demonstrates the high potential for applying zircon and apatite petrochronology in eclogites in reconstruction of the metamorphic histories of (U)HP terranes. Future studies should consider further petrochronology of eclogites, particularly that of apatite, to improve the dataset required to complete tectono-metamorphic history of the Scandinavian Caledonides, specifically their retrogressive stages reflected in apatite U–Pb age record. Nonetheless, the combined use of coupled trace element and U–Pb analyses of zircon and apatite has proven its potential to resolve the prograde, peak, and retrogressive metamorphic evolution of eclogites, highlighting the necessity of analyzing trace element compositions when dating zircon grains as well as introducing the capabilities of apatite petrochronology in eclogite studies.

Supplementary Information The online version contains supplementary material available at https://doi.org/10.1007/s00410-023-02029-5.

Acknowledgements S. Cuthbert, I. Klonowska and M. Bukała are thanked for their efforts during fieldwork and sample collection. Insightful and valuable comments from editor O. Müntener, reviewer D. Chew and anonymous reviewer are greatly appreciated. I. Kocjan, A. Zagórska and T. Siwecki are acknowledged for the assistance with sample preparation.

Funding This study was funded by IGS PAS research project "Petrochron".

Data availability All data related to this work are presented in the article and supplementary material.

Declarations

Conflict of interest The authors declare that there are no known conflicts of interest that have affected data acquisition or presented interpretations.

References

Andréasson PG (1994) The Baltoscandian margin in neoproterozoic-early palaeozoic times. Some constraints on terrane derivation and accretion in the Arctic Scandinavian Caledonides. Tectonophysics 231:1–32. https://doi.org/10.1016/0040-1951(94)90118-X

Bender H, Ring U, Almqvist BSG, Grasemann B, Stephens MB (2018) Metamorphic zonation by out-of-sequence thrusting at back-stepping subduction zones: Sequential accretion of the Caledonian internides, central Sweden. Tectonics 37:3545–3576. https://doi.org/10.1029/2018TC005088

Bender H, Glodny J, Ring U (2019) Absolute timing of Caledonian orogenic wedge assembly, Central Sweden, constrained by Rb–Sr multi-mineral isochron data. Lithos 344–345:339–359. https://doi.org/10.1016/j.lithos.2019.06.033

Bingen B, Demaiffe D, Hertogen J (1996) Redistribution of rare earth elements, thorium, and uranium over accessory minerals in the course of amphibolite to granulite facies metamorphism: the role of apatite and monazite in orthogneisses from southwestern Norway. Geochim Cosmochim Acta 60:1341–1354. https://doi.org/10.1016/0016-7037(96)00006-3

Bingen B, Austrheim H, Whitehouse MJ, Davis WJ (2004) Trace element signature and U-Pb geochronology of eclogite-facies zircon, Bergen Arcs, Caledonides of W Norway. Contrib Mineral Petrol 147:671–683. https://doi.org/10.1007/s00410-004-0585-z

Bloch EM, Jollands MC, Devoir A, Bouvier AS, Ibañez-Mejia M, Baumgartner LP (2020) Multispecies diffusion of yttrium, rare

earth elements and hafnium in garnet. J Petrol 61:7egaa055. https://doi.org/10.1093/petrology/egaa055
Brueckner HK (2006) Dunk, dunkless and re-dunk tectonics: a model for metamorphism, lack of metamorphism, and repeated metamorphism of HP/UHP terranes. Int Geol Rev 48:978–995. https://doi.org/10.2747/0020-6814.48.11.978
Brueckner HK, Van Roermund HLM (2007) Concurrent HP metamorphism on both margins of Iapetus: ordovician ages for eclogites and garnet pyroxenites from the Seve Nappe Complex, Swedish Caledonides. J Geol Soc London 164:117–128. https://doi.org/10.1144/0016-76492005-139
Brueckner HK, van Roermund HLM, Pearson NJ (2004) An Archean (?) to Paleozoic evolution for a garnet peridotite lens with subbaltic shield affinity within the Seve Nappe Complex of Jämtland, Sweden, Central Scandinavian Caledonides. J Petrol 45:415–437. https://doi.org/10.1093/petrology/egg088
Bukała M, Klonowska I, Barnes C, Majka J, Kośmińska K, Janák M, Fassmer K, Broman C, Luptáková J (2018) UHP metamorphism recorded by phengite eclogite from the Caledonides of northern Sweden: P–T path and tectonic implications. J Metamorph Geol 36:547–566. https://doi.org/10.1111/jmg.12306
Carswell DA, Brueckner HK, Cuthbert SJ, Mehta K, O'Brien PJ (2003) The timing of stabilisation and the exhumation rate for ultra-high pressure rocks in the Western Gneiss Region of Norway. J Metamorph Geol 21:601–612. https://doi.org/10.1046/j.1525-1314.2003.00467.x
Chen JF, Han BF, Ji JQ, Zhang L, Xu Z, He GQ, Wang T (2010) Zircon U-Pb ages and tectonic implications of Paleozoic plutons in northern West Junggar, North Xinjiang, China. Lithos 115:137–152. https://doi.org/10.1016/j.lithos.2009.11.014
Cherniak DJ (2000) Rare earth element diffusion in apatite. Geochim Cosmochim Acta 64:3871–3885. https://doi.org/10.1016/S0016-7037(00)00467-1
Cherniak DJ (2010) Diffusion in accessory minerals: Zircon, titanite, apatite, monazite and xenotime. Rev Mineral Geochemistry 72:827–869. https://doi.org/10.2138/rmg.2010.72.18
Cherniak DJ, Lanford WA, Ryerson FJ (1991) Lead diffusion in apatite and zircon using ion implantation and Rutherford Backscattering techniques. Geochim Cosmochin Acta 55:1663–1673. https://doi.org/10.1016/0016-7037(91)90137-T
Chew DM, Spikings RA (2015) Geochronology and thermochronology using apatite: time and temperature, lower crust to surface. Elements 11:189–194. https://doi.org/10.2113/gselements.11.3.189
Chew DM, Sylvester PJ, Tubrett MN (2011) U-Pb and Th-Pb dating of apatite by LA-ICPMS. Chem Geol 280:200–216. https://doi.org/10.1016/j.chemgeo.2010.11.010
Corfu F (2004) U-Pb age, setting and tectonic significance of the anorthosite-mangerite-charnockite-granite suite, Lofoten-Vesterålen, Norway. J Petrol 45:1799–1819. https://doi.org/10.1093/petrology/egh034
Corfu F, Ravna EJK, Kullerud K (2003a) A late ordovician U-Pb age for the Tromsø Nappe eclogites uppermost allochthon of the Scandinavian Caledonides. Contrib to Mineral Petrol 145:502–513. https://doi.org/10.1007/s00410-003-0466-x
Corfu F, Andersen TB, Gasser D (2014) The Scandinavian Caledonides: main features, conceptual advances and critical questions. Geol Soc Spec Publ 390:9–43. https://doi.org/10.1144/SP390.25
Corfu F, Hanchar JM, Hoskin PWO, Kinny P (2003b) Atlas of zircon textures. In: Hanchar JM, Hoskin PWO (eds) Zircon. Reviews in Mineralogy and Geochemistry 53:469–500
Cuthbert SJ, Carswell DA, Krogh-Ravna EJ, Wain A (2000) Eclogites and eclogites in the Western Gneiss region, Norwegian Caledonides. Lithos 52:165–195. https://doi.org/10.1016/S0024-4937(99)00090-0
Cuthbert SJ, van Roermund, HLM (2011). In-situ monazite dating of a microdiamond-bearing gneiss, Fjortoft, Norway: Age pattern in relation to garnet zoning and growth history. 9th Internation Eclogite Conference 2011
Cutts JA, Smit MA (2018) Rates of deep continental burial from Lu-Hf garnet chronology and Zr-in-Rutile thermometry on (Ultra)high-pressure rocks. Tectonics 37:71–88. https://doi.org/10.1002/2017TC004723
Dobrzhinetskaya LF (1995) Microdiamond in high-grade metamorphic rocks of the Western Gneiss region, Norway. Geology 23:597–600. https://doi.org/10.1130/0091-7613(1995)023%3c0597:MIHGMR%3e2.3.CO;2
Fassmer K, Klonowska I, Walczak K, Andersson B, Froitzheim N, Majka J, Fonseca POC, Münker C, Janák M, Whitehouse M (2017) Middle Ordovician subduction of continental crust in the Scandinavian Caledonides: an example from Tjeliken, Seve Nappe Complex, Sweden. Contrib Mineral Petrol. https://doi.org/10.1007/s00410-017-1420-7
Fassmer K, Froitzheim N, Janák M, Strohmeyer M, Bukała M, Lagos M, Münker C (2021) Diachronous collision in the Seve Nappe Complex: evidence from Lu–Hf geochronology of eclogites (Norrbotten, North Sweden). J Metamorph Geol 39:819–842. https://doi.org/10.1111/jmg.12591
Ferry JM, Watson EB (2007) New thermodynamic models and revised calibrations for the Ti-in-zircon and Zr-in-rutile thermometers. Contrib Mineral Petrol 154:429–437. https://doi.org/10.1007/s00410-007-0201-0
Fleet ME, Pan Y (1995) Site preference of rare earth elements in fluorapatite. Am Mineral 80(3–4):329–335. https://doi.org/10.2138/am-1995-3-414
Fournier HW, Lee JKW, Camacho A, Creaser RA (2014) Retrogression of eclogite-facies shear zones by short-lived fluid infiltration during the Caledonian orogeny, Lofoten Islands, Norway. Geol Soc Spec Publ 390:443–466. https://doi.org/10.1144/SP390.9
Fournier HW, Lee JKW, Camacho A (2019) Slow cooling versus episodic fluid injections: deciphering the Caledonian orogeny in Vestvågøy, Lofoten islands, Norway. J Metamorph Geol 37:769–793. https://doi.org/10.1111/jmg.12485
Froitzheim N, Miladinova I, Janák M, Kullerud K, Ravna EK, Majka J, Fonseca ROC, Münker C, Nagel TJ (2016) Devonian subduction and syncollisional exhumation of continental crust in Lofoten, Norway. Geology 44:223–226. https://doi.org/10.1130/G37545.1
Gee D (1975) A tectonic model for the central part of the Scandinavian Caledonides. Am J Sci 275:468–515
Gee DG, Sturt BA (1985) The caledonide orogeny—Scandinavia and related areas. Wiley, Chichester
Gee DG, Janák M, Majka J, Robinson P, van Roermund HLM (2013) Subduction along and within the baltoscandian margin during closing of the lapetus ocean and baltica-laurentia collision. Lithosphere 5:169–178. https://doi.org/10.1130/L220.1
Gee DG, Ladenberger A, Dahlqvist P, Majka J, Beeri-Shlevin Y, Frei D, Thomsen T (2014) The Baltoscandian margin detrital zircon signatures of the central Scandes. Geol Soc Spec Publ 390:131–155. https://doi.org/10.1144/SP390.20
Gee DG, Andréasson PG, Lorenz H, Frei D, Majka J (2015) Detrital zircon signatures of the Baltoscandian margin along the Arctic Circle Caledonides in Sweden: the Sveconorwegian connection. Precambrian Res 265:40–56. https://doi.org/10.1016/j.precamres.2015.05.012
Gee DG, Fossen H, Henriksen N, Higgins AK (2008) From the early Paleozoic platforms of Baltica and Laurentia to the Caledonide Orogen of Scandinavia and Greenland. Episodes 31:44–51. https://doi.org/10.18814/epiiugs/2008/v31i1/007
Gieré R, Sorensen SS (2004) Allanite and other REE-rich epidote-group minerals. Rev Mineral Geochem 56:431–493. https://doi.org/10.2138/gsrmg.56.1.431

Gilio M, Clos F, van Roermund HLM (2015) The Friningen Garnet Peridotite (central Swedish Caledonides). A good example of the characteristic PTt path of a cold mantle wedge garnet peridotite. Lithos 230:1–16. https://doi.org/10.1016/j.lithos.2015.05.003

Gilio M, Scambelluri M, Angel RJ, Alvaro M (2021) The contribution of elastic geothermobarometry to the debate on HP versus UHP metamorphism. J Metamorph Geol. https://doi.org/10.1111/jmg.12625

Grauch RI (1989) Rare earth elements in metamorphic rocks. In: Lipin BR, McKay GA (eds) Geochemistry and mineralogy of rare earth elements. Reviews in Mineralogy 21:147–167

Griffin WL, Taylor PN, Hakkinen JW, Heier KS, Iden IK, Krogh EJ, Maim O, Olsen KI, Ormaasen DE, Tveten E (1978) Archaean and Proterozoic crustal evolution in Lofoten-Vesterålen, N Norway. J Geol Soc 135:629–647

Grimmer JC, Glodny J, Drüppel K, Greiling RO, Kontny A (2015) Early- to mid-Silurian extrusion wedge tectonics in the central Scandinavian Caledonides. Geology 43:347–350. https://doi.org/10.1130/G36433.1

Hacker BR, Gans PB (2005) Continental collisions and the creation of ultrahigh-pressure terranes: petrology and thermochronology of nappes in the central Scandinavian Caledonides. Bull Geol Soc Am 117:117–134. https://doi.org/10.1130/B25549.1

Hacker BR, Andersen TB, Johnston S, Kylander-Clark ARC, Peterman EM, Walsh EO, Young D (2010) High-temperature deformation during continental-margin subduction & exhumation: the ultrahigh-pressure Western Gneiss Region of Norway. Tectonophysics 480:149–171. https://doi.org/10.1016/j.tecto.2009.08.012

Harley SL, Kelly NM, Möller A (2007) Zircon behaviour and the thermal histories of moutain chains. Elements 3:25–30. https://doi.org/10.2113/gselements.3.1.25

Harlov DE (2015) Apatite: a fingerprint for metasomatic processes. Elements 11:171–176. https://doi.org/10.2113/gselements.11.3.171

Harlov DE, Förster H-J (2003) Fluid-induced nucleation of (Y+REE)-phosphate minerals within apatite: nature and experiment. Part II. Fluorapatite. Am Mineral 88:1209–1229. https://doi.org/10.2138/am-2003-8-905

Henrichs IA, O'Sullivan G, Chew DM, Mark C, Babechuk MG, McKenna C, Emo R (2018) The trace element and U-Pb systematics of metamorphic apatite. Chem Geol 483:218–238. https://doi.org/10.1016/j.chemgeo.2017.12.031

Henrichs IA, Chew DM, O'Sullivan GJ, Mark C, McKenna C, Guyett P (2019) Trace element (Mn-Sr-Y-Th-REE) and U-Pb isotope systematics of metapelitic apatite during progressive greenschist- to amphibolite-facies Barrovian metamorphism. Geochem Geophys Geosyst 20:4103–4129. https://doi.org/10.1029/2019GC008359

Holder RM, Hacker BR, Kylander-Clark ARC, Cottle JM (2015) Monazite trace-element and isotopic signatures of (ultra)high-pressure metamorphism: examples from the Western Gneiss Region, Norway. Chem Geol 409:99–111. https://doi.org/10.1016/j.chemgeo.2015.04.021

Hollocher K, Robinson R, Van Nostrand M, Walsh E (2022) The Blåhø Nappe, central Norwegian Scandinavian Caledonides: An oceanic arc–back-arc assemblage distinct from the Seve Nappe Complex. In: Kuiper YD, Murphy JB, Nance RD, Strachan RA, Thompson MD (eds) New Developments in the Appalachian-Caledonian-Variscan Orogen: Geological Society of America Special Paper 554:315–334. https://doi.org/10.1130/2022.2554(13)

Horstwood MSA, Košler J, Gehrels G, Jackson SE, McLean NM, Paton C, Pearson NJ, Sircombe K, Sylvester P, Vermeesch P, Bowring JF, Condon DJ, Schoene B (2016) Community-derived standards for LA-ICP-MS U-(Th-)Pb geochronology—uncertainty propagation, age interpretation and data reporting. Geostand Geoanal Res 40:311–332. https://doi.org/10.1111/j.1751-908X.2016.00379.x

Hoskin PWO, Black LP (2000) Metamorphic zircon formation by solid-state recrystallization of protolith igneous zircon. J Metamorph Geol 18:423–439. https://doi.org/10.1046/j.1525-1314.2000.00266.x

Janák M, Van Roermund H, Majka J, Gee D (2013) UHP metamorphism recorded by kyanite-bearing eclogite in the Seve Nappe Complex of northern Jämtland, Swedish Caledonides. Gondwana Res 23:865–879. https://doi.org/10.1016/j.gr.2012.06.012

Jepson G, Carrapa B, George SWM, Triantafyllou A, Egan SM, Constenius KN, Gehrels GE, Ducea MN (2021) Resolving mid- to upper-crustal exhumation through apatite petrochronology and thermochronology. Chem Geol 565:120071. https://doi.org/10.1016/j.chemgeo.2021.120071

Kelly NM, Harley SL (2005) An integrated microtextural and chemical approach to zircon geochronology: refining the Archaean history of the Napier Complex, east Antarctica. Contrib Mineral Petrol 149:57–84. https://doi.org/10.1007/s00410-004-0635-6

Ketcham RA (2015) Technical Note: Calculation of stoichiometry from EMP data for apatite and other phases with mixing on monovalent anion sites. Am Mineral 100:1620–1623. https://doi.org/10.2138/am-2015-5171

Klonowska I, Janák M, Majka J, Froitzheim N, Kośmińska K (2016) Eclogite and garnet pyroxenite from Stor Jougdan, Seve Nappe Complex, Sweden: implications for UHP metamorphism of allochthons in the Scandinavian Caledonides. J Metamorph Geol 34:103–119. https://doi.org/10.1111/jmg.12173

Kohn MJ, Corrie SL, Markley C (2015) The fall and rise of metamorphic zircon. Am Mineral 100:897–908. https://doi.org/10.2138/am-2015-5064

Kooijman E, Mezger K, Berndt J (2010) Constraints on the U-Pb systematics of metamorphic rutile from in situ LA-ICP-MS analysis. Earth Planet Sci Lett 293:321–330. https://doi.org/10.1016/j.epsl.2010.02.047

Krause J, Harlov DE, Pushkarev EV, Brügmann GE (2013) Apatite and clinopyroxene as tracers for metasomatic processes in nepheline clinopyroxenites of Uralian-Alaskan-type complexes in the Ural Mountains, Russian Federation. Geochim Cosmochim Acta 121:503–521. https://doi.org/10.1016/j.gca.2013.06.013

Krogh TE, Kamo SL, Robinson P, Terry MP, Kwok K (2011) U-Pb zircon geochronology of eclogites from the Scandian Orogen, Northern Western Gneiss Region, Norway: 14–20 million years between eclogite crystallization and return to amphibolitefacies conditions. Can J Earth Sci 48:441–472. https://doi.org/10.1139/E10-076

Kullerud K (1995) Chlorine, titanium and barium-rich biotites: factors controlling biotite composition and the implications for garnet-biotite geothermometry. Contrib Mineral Petrol 120:42–59. https://doi.org/10.1007/BF00311007

Kullerud K (1996) Chlorine-rich amphiboles: interplay between amphibole composition and an evolving fluid. Eur J Mineral 8:355–370. https://doi.org/10.1127/ejm/8/2/0355

Kullerud K, Erambert M (1999) Cl-scapolite, Cl-amphibole, and plagioclase equilibria in ductile shear zones at Nusfjord, Lofoten, Norway: Implications for fluid compositional evolution during fluid-mineral interaction in the deep crust. Geochim Cosmochim Acta 63:3829–3844. https://doi.org/10.1016/S0016-7037(99)00150-7

Kullerud K, Stephens MB, Zachrisson E (1990) Pillow lavas as protoliths for eclogites: evidence from a late Precambrian-Cambrian continental margin, Seve Nappes, Scandinavian Caledonides. Contrib Mineral Petrol 105:1–10. https://doi.org/10.1007/BF00320962

Kullerud K (1992) Metamorphism and fluid–rock interaction in shear zones within the Flakstadøy Basic Complex, Lofoten, Northern Norway. Ph.D. thesis, University of Oslo

Kylander-Clark ARC, Hacker BR, Johnson CM, Beard BL, Mahlen NJ (2009) Slow subduction of a thick ultrahigh-pressure terrane. Tectonics 28:1–14. https://doi.org/10.1029/2007TC002251

Kylander-Clark ARC, Hacker BR (2014) Age and significance of felsic dikes from the UHP western gneiss region. Tectonics 33:2342–2360. https://doi.org/10.1002/2014TC003582

Litjens A (2002) PT estimates of high-pressure metamorphic rocks from the Seve Nappe complex, Jämtland, Central Scandinavian Caledonides. MSc thesis, University of Utrecht

Liu P, Massonne HJ (2019) An anticlockwise P–T–t path at high-pressure, high-temperature conditions for a migmatitic gneiss from the island of Fjørtoft, Western Gneiss Region, Norway, indicates two burial events during the Caledonian orogeny. J Metamorph Geol 37:567–588. https://doi.org/10.1111/jmg.12476

Liu P, Massonne HJ (2022) High-pressure granulite facies re-equilibration and zoisite–biotite dehydration melting during decompression of an ultrahigh-pressure garnet clinopyroxenite from the island of Fjørtoft, Norway. J Metamorph Geol 40(5):887–918. https://doi.org/10.1111/jmg.12649

Ludwig KR (2012) Isoplot 4.15: a geochronological toolkit for Microsoft Excel. Berkeley Geochronology Center Special Publication 5

Majka J, Janák M, Andersson B, Klonowska I, Gee DG, Rosén Å, Kośmińska K (2014) Pressure-temperature estimates on the Tjeliken eclogite: new insights into the (ultra)-high-pressure evolution of the Seve Nappe Complex in the Scandinavian Caledonides. Geol Soc Spec Publ 390:369–384. https://doi.org/10.1144/SP390.14

March S, Hand M, Tamblyn R, Carvalho BB, Clark C (2022) A diachronous record of metamorphism in metapelites of the Western Gneiss Region, Norway. J Metamorph Geol 40:1121–1158. https://doi.org/10.1111/jmg.12660

Markl G, Bucher K (1997) Proterozoic eclogites from the Lofoten islands, northern Norway. Lithos 42:15–35. https://doi.org/10.1016/s0024-4937(97)00034-0

McDonough WF, Sun SS (1995) The composition of the Earth. Chem Geol 120:223–253. https://doi.org/10.1016/0009-2541(94)00140-4

O'Sullivan GJ, Chew DM, Morton AC, Mark C, Henrichs IA (2018) An integrated apatite geochronology and geochemistry tool for sedimentary provenance analysis. Geochem Geophys Geosyst 19:1309–1326. https://doi.org/10.1002/2017GC007343

O'Sullivan G, Chew D, Kenny G, Henrichs IA, Mulligan D (2020) The trace element composition of apatite and its application to detrital provenance studies. Earth-Science Rev 201:103044. https://doi.org/10.1016/j.earscirev.2019.103044

Pan Y, Fleet ME (2002) Compositions of the apatite-group minerals: substitution mechanisms and controlling factors. Rev Mineral Geochem 48:13–50. https://doi.org/10.2138/rmg.2002.48.2

Petrík I, Janák M, Klonowska I, Majka J, Froitzheim N, Yoshida K, Sasinková V, Konečný P, Vaculovič T (2019) Monazite behaviour during metamorphic evolution of a diamond-bearing gneiss: a case study from the Seve Nappe Complex, Scandinavian Caledonides. J Petrol 60:1773–1796. https://doi.org/10.1093/petrology/egz051

Piccoli PM, Candela PA (2002) Apatite in igneous systems. Rev Mineral Geochem 48:255–292. https://doi.org/10.2138/rmg.2002.48.6

Roberts D, Stephens MB (2000) Caledonian orogenic belt. Description to the Bedrock Map of Central Fennoscandia (Mid-Norden). Geol Surv Finl Spe Papers 28:79–108

Van Roermund HLM (1985) Eclogites from the Seve Nappe, Central Scandinavian Caledonides, in The Caledonide Orogeny—Scandinavia and Related Areas, edited by D. G. Gee and B. A. Sturt, pp 873–886

Root D, Corfu F (2012) U-Pb geochronology of two discrete Ordovician high-pressure metamorphic events in the Seve Nappe Complex, Scandinavian Caledonides. Contrib Mineral Petrol 163:769–788. https://doi.org/10.1007/s00410-011-0698-0

Rubatto D (2002) Zircon trace element geochemistry: partitioning with garnet and the link between U-Pb ages and metamorphism. Chem Geol 184:123–138. https://doi.org/10.1016/S0009-2541(01)00355-2

Rubatto D (2017) Zircon: the Metamorphic Mineral. Rev Mineral Geochem 83:261–289. https://doi.org/10.2138/rmg.2017.83.9

Rubatto D, Hermann J (2007) Experimental zircon/melt and zircon/garnet trace element partitioning and implications for the geochronology of crustal rocks. Chem Geol 241:38–61. https://doi.org/10.1016/j.chemgeo.2007.01.027

Schettler G, Gottschalk M, Harlov DE (2011) A new semi-micro wet chemical method for apatite analysis and its application to the crystal chemistry of fluorapatite-chlorapatite solid solutions. Am Mineral 96:138–152. https://doi.org/10.2138/am.2011.3509

Sha LK, Chappell BW (1999) Apatite chemical composition, determined by electron microprobe and laser-ablation inductively coupled plasma mass spectrometry, as a probe into granite petrogenesis. Geochim Cosmochim Acta 63:3861–3881. https://doi.org/10.1016/S0016-7037(99)00210-0

Simpson A, Gilbert S, Tamblyn R, Hand M, Spandler C, Gillespie J, Nixon A, Glorie S (2021) In-situ Lu Hf geochronology of garnet, apatite and xenotime by LA ICP MS/MS. Chem Geol 577:120299. https://doi.org/10.1016/j.chemgeo.2021.120299

Smit MA, Scherer EE, Bröcker M, van Roermund HLM (2010) Timing of eclogite facies metamorphism in the southernmost Scandinavian Caledonides by Lu-Hf and Sm-Nd geochronology. Contrib Mineral Petrol 159:521–539. https://doi.org/10.1007/s00410-009-0440-3

Spear FS, Pyle JM (2002) Apatite, monazite, and xenotime in metamorphic rocks. Rev Mineral Geochem 48:293–336. https://doi.org/10.2138/rmg.2002.48.7

Steltenpohl M, Hames W, Andresen A, Markl G (2003) New Caledonian eclogite province in Norway and potential Laurentian (Taconic) and Baltic links. Geology 31:985–988. https://doi.org/10.1130/G19744.1

Steltenpohl MG, Hames WE, Andresen A (2004) The Silurian to Permian history of a metamorphic core complex in Lofoten, northern Scandinavian Caledonides. Tectonics 23:1–23. https://doi.org/10.1029/2003TC001522

Steltenpohl MG, Kassos G, Andresen A (2006) Retrograded eclogite-facies pseudotachylytes as deep-crustal paleoseismic faults within continental basement of Lofoten, North Norway. Geosphere 2:61–72. https://doi.org/10.1130/GES00035.1

Steltenpohl MG, Kassos G, Andresen A, Rehnström EF, Hames WE (2011a) Eclogitization and exhumation of Caledonian continental basement in Lofoten, North Norway. Geosphere 7:202–218. https://doi.org/10.1130/GES00573.1

Steltenpohl MG, Moecher D, Andresen A, Ball J, Mager S, Hames WE (2011b) The Eidsfjord shear zone, Lofoten-Vesterålen, north Norway: an early Devonian, paleoseismogenic low-angle normal fault. J Struct Geol 33:1023–1043. https://doi.org/10.1016/j.jsg.2011.01.017

Stephens MB, Gee DG (1989) Terranes and polyphase accretionary history in the Scandinavian Caledonides, in R.D. Dallmeyer ed., Terranes in the Circum-Atlantic Paleozoic Orogens: Geological Society of America. Geol Soc Am Spec Pap 17–30

Stephens MB, Gee DG, Sturt BA (1985) A tectonic model for the evolution of the eugeoclinal terranes in the central Scandinavian Caledonides in the Caledonide Orogen: Scandinavia and Related Areas edited by D. G. Gee and B. A. Sturt, pp 953–978

Strömberg AGB, Karis L, Zachrisson E, Sjöstrand T, Skogland R (1984). Bedrock Geological Map of Jämtland County (Caledonides), scale 1:200 000. Sveriges Geologiska Undersökning, Uppsala, Sweden, Ca 53

Tamblyn R, Hand M, Simpson A, Gilbert S, Wade B, Glorie S (2022) In situ laser ablation Lu–Hf geochronology of garnet across the Western Gneiss Region: campaign-style dating of metamorphism. J Geol Soc Lond. https://doi.org/10.1144/jgs2021-094

Terry MP, Robinson P (2003) Evolution of amphibolite-facies structural features and boundary conditions for deformation during exhumation of high- and ultrahigh-pressure rocks, Nordøyane, Western Gneiss Region, Norway. Tectonics 22:1–23. https://doi.org/10.1029/2001tc001349

Terry MP, Robinson P (2004) Geometry of eclogite-facies structural features: Implications for production and exhumation of ultrahigh-pressure and high-pressure rocks, Western Gneiss Region, Norway. Tectonics 23:1–23. https://doi.org/10.1029/2002TC001401

Terry MP, Robinson P, Hamilton MA, Jercinovic MJ (2000a) Monazite geochronology of UHP and HP metamorphism, deformation, and exhumation Nordøyane, Western Gneiss Region, Norway. Am Mineral 85:1651–1664. https://doi.org/10.2138/am-2000-11-1208

Terry MP, Robinson P, Krogh Ravna EJ (2000b) Kyanite eclogite thermobarometry and evidence for thrusting of UHP over HP metamorphic rocks, Nordoyane, Western Gneiss Region, Norway. Am Mineral 85:1637–1650. https://doi.org/10.2138/am-2000-11-1207

Torsvik TH, Cocks LRM (2005) Norway in space and time: a Centennial cavalcade. Nor Geol Tidsskr 85:73–86

Trouw RAJ (1973) Structural geology of the Caledonides of Västerbotten. Sveriges Geol Unders 689:1–115

Tual L, Smit MA, Kooijman E, Kielman-Schmitt M, Ratschbacher L (2022) Garnet, zircon, and monazite age and REE signatures in (ultra)high-temperature and high-pressure rocks: examples from the Caledonides and the Pamir. J Metamorph Geol 40(8):1321–1346. https://doi.org/10.1111/jmg.12667

Van Roermund HLM (1989) High-pressure ultramafic rocks from the allochthonous nappes of the Swedish Caledonides. Caledonide Geol Scand. https://doi.org/10.1007/978-94-009-2549-6_17

Walczak K, Cuthbert S, Kooijman E, Majka J, Smit MA (2019) U-Pb zircon age dating of diamond-bearing gneiss from Fjørtoft reveals repeated burial of the Baltoscandian margin during the Caledonian Orogeny. Geol Mag. https://doi.org/10.1017/S0016756819000268

Walsh E, Hacker BR, Gans PB, Wong MS, Andersen TB (2013) Crustal exhumation of the Western Gneiss Region UHP terrane, Norway: $^{40}Ar/^{39}Ar$ thermochronology and fault-slip analysis. Tectonophysics 608:1159–1179. https://doi.org/10.1016/j.tecto.2013.06.030

Whitehouse MJ, Platt JP (2003) Dating high-grade metamorphism—constraints from rare-earth elements in zircon and garnet. Contrib Mineral Petrol 145:61–74. https://doi.org/10.1007/s00410-002-0432-z

Williams PF, Zwart HJ (1977) A Model for the development of the Seve-Köli Caledonian Nappe complex. In: Saxena SK, Bhattacharji S, Annersten H, Stephansson O (eds) Energetics of geological processes. Springer, Berlin

Zachrisson E, Sjöstrand T (1990) Bedrock map 22E Frostviken, 1:50 000. Sveriges Geologiska Undersökning, Uppsala, Ai, 44

Zhu C, Sverjensky DA (1991) Partitioning of F–Cl–OH between minerals and hydrothermal fluids. Geochim Cosmochim Acta 55:1837–1858. https://doi.org/10.1016/0016-7037(91)90028-4